

# Giant atoms coupled to waveguide: Continuous coupling and multiple excitations

Shiying Lin,<sup>1,2</sup> Xinyu Zhao,<sup>1,2,\*</sup> and Yan Xia<sup>1,2,†</sup>

<sup>1</sup>*Fujian Key Laboratory of Quantum Information and Quantum Optics (Fuzhou University), Fuzhou 350116, China*

<sup>2</sup>*Department of Physics, Fuzhou University, Fuzhou 350116, China*

We propose a stochastic Schrödinger equation (SSE) approach to investigate the dynamics of giant atoms coupled to a waveguide, addressing two critical gaps in existing research, namely insufficient exploration on continuous coupling and multiple excitations. A key finding is that continuous coupling, unlike discrete coupling at finite points, breaks the constant phase difference condition, thereby weakening the interference effects in giant atom-waveguide systems. In addition, a key technical advantage of the SSE approach is that auto- and cross-correlation functions can directly reflect the complex photon emission/absorption processes and time-delay effects in giant atom-waveguide systems. Moreover, the SSE approach also naturally handles multiple excitations, without increasing equation complexity as the number of excitations grows. This feature enables the investigation of multi-excitation initial states of the waveguide, such as thermal and squeezed initial states. Overall, our approach provides a powerful tool for studying the dynamics of giant atoms coupled to waveguide, particularly for continuous coupling and multi-excitation systems.

## I. INTRODUCTION

In recent years, artificial giant atoms have attracted the attention of many researchers due to their unique properties [1–16]. Since the size of giant atoms cannot be ignored, the coupling between giant atoms and light fields can be more complicated [8, 17, 18]. In particular, when giant atoms are coupled to a waveguide, a series of novel physical phenomena emerge due to interference and time-delay effects that do not occur in small atom systems [19–31]. For example, the complicated interaction between waveguide and giant atoms leads to collective enhancement and interference [32–34], frequency-dependent Lamb shift and relaxation [11], single-photon scattering [2, 12, 35–38], and decoherence-free interaction [8, 19, 39–41]. Additionally, it also induces non-Markovian decay dynamics [40, 42, 43], novel bound states [12, 44–47], phase regulation and photon shielding [12, 48].

All these novel phenomena related to giant atoms fundamentally originate from the interference effects in the photon emission and absorption process. [2, 33, 34, 49, 50]. As shown in Fig. 1(a), in the case of small atoms coupled to waveguide, photons emitted by an atom can be only absorbed by other atoms at fixed positions, with deterministic phase accumulation [51, 52]. In contrast, as shown in Fig. 1(c), giant atoms enable photon emission from arbitrary point in a continuous region, followed by potential reabsorption at arbitrary point in a continuous region [10, 19, 35, 49, 53–56]. This complex photon emission and absorption process greatly enriches the interference effects among various possible paths. [1, 5, 42, 44, 57]. However, two critical gaps remain in existing research, limiting our understanding of giant atom-waveguide dynamics.

### Gap 1: Rarely explored continuous coupling

Existing studies have predominantly focused on two (or a few) discrete coupling points as shown in Fig. 1(b) [12, 19, 58, 59], leaving the novel physics induced by continuous coupling [Fig. 1(c)] rarely discussed.

As we have discussed, all interesting phenomena in giant atom systems stem from interference effects [1, 9, 14, 17, 34]. When there are only a few discrete coupling [(e.g., two coupling points as shown in Fig. 1(b))], the phase difference is essentially fixed, leading to strong constructive and destructive interference. In the case of continuous coupling points shown in Fig. 1(c), however, this condition of constant phase difference is broken, which inevitably weakens the interference effects. Exploring how the broadening of the coupling region influences the dynamics of giant atoms constitutes a valuable research topic.

### Gap 2: Rarely addressed multiple excitation effects

In many studies, the dynamical equations are obtained by assuming single excitation in the initial state to limit the Hilbert space to finite dimensions [4, 13, 55, 58] (see discussion in Sec. III). But the multiple excitation effect [60] is rarely discussed, particularly for the multi-photon initial states in the waveguide.

Notably, waveguides support a complete continuum of modes, including ultra-low-frequency modes with vanishingly small energies. At finite temperatures, the thermal occupation of these low-frequency modes becomes non-negligible. Therefore, the single-excitation assumption is invalid in practical cases. Hence, studying multiple excitation effects is essential to capture the realistic dynamics of giant atoms.

In this paper, inspired by the non-Markovian quantum state diffusion method in the theory of open quantum systems [61–74], we propose an alternative approach, the stochastic Schrödinger equation (SSE) approach, to derive the dynamical equations governing the time evolution of giant atoms. By expanding the quantum states of the waveguide in coherent state basis, we derive the SSE and the corresponding master equation from the

\* [xzhao@fzu.edu.cn](mailto:xzhao@fzu.edu.cn)

† [xia-208@163.com](mailto:xia-208@163.com)

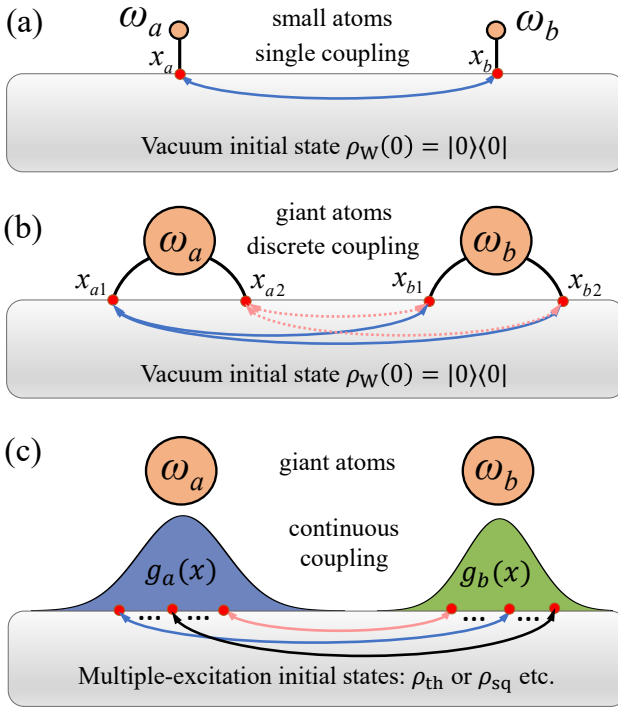


FIG. 1. Schematic diagram of the two giant atoms (labeled “a” and “b”) coupled to a waveguide. (a) Single coupling (small atom) with vacuum initial state of the waveguide. (b) Discrete coupling (two coupling points) with vacuum initial state of the waveguide. (c) Continuous coupling with multiple-excitation (e.g. thermal or squeezed) initial states of the waveguide.

original Hamiltonian without introducing phenomenological treatments. The proposed theoretical framework enables the investigation beyond single-excitation state, while simultaneously offering complete characterization of multiple-excited initial states including thermal [75] and squeezed states [76] in the waveguide.

With the SSE approach, we systematically investigate how the continuous coupling affects the quantum dynamics of giant atoms in a waveguide. A notable advantage of the SSE approach is that the correlation functions intuitively capture photon emission and absorption processes, which serves as a powerful tool to analyze the time-delayed effects. Our numerical results show that continuous coupling with a single-peak Gaussian distribution enables more photon emission and absorption paths, thereby enhancing of entanglement generation.

As the most important result of this work, it should be highlighted that continuous coupling between giant atoms and the waveguide over a region (rather than discrete coupling at several specific points) leads to complex photon emission-absorption processes with diverse propagation times, which breaks the constant phase difference condition. Since this condition is essential for interference effects, continuous coupling may compromise

the performance of most established applications of giant atoms relying on interference.

Finally, we extend our analysis beyond the single-excitation subspace. For double-excitation states, we analyze the influence of the distribution width on entanglement dynamics and explain the reason through photon emission and absorption picture. Last but not least, we demonstrate that our approach is applicable to the multi-photon initial states, including thermal and squeezed initial states of the waveguide.

## II. THE MODEL: GIANT ATOMS COUPLED TO WAVEGUIDE

As shown in Fig. 1(c), we consider two giant atoms coupled to a waveguide as an example. The total Hamiltonian (setting  $\hbar = 1$ ) is given by

$$H_{\text{tot}} = H_A + H_W + H_{\text{int}}, \quad (1)$$

$$H_A = \sum_{\mu=a,b} \omega_{\mu} \sigma_{\mu}^{+} \sigma_{\mu}^{-}, \quad (2)$$

$$H_W = \sum_k \omega_k c_k^{\dagger} c_k, \quad (3)$$

$$H_{\text{int}} = \sum_{\mu=a,b} \sum_k \left( G_{\mu k} c_k^{\dagger} \sigma_{\mu}^{-} + \text{H.c.} \right), \quad (4)$$

where  $H_A$ ,  $H_W$ , and  $H_{\text{int}}$  indicate the Hamiltonian for two giant atoms, the waveguide, and their interaction, respectively. The transition frequencies for two giant atoms “a” and “b” are described by  $\omega_{\mu}$  ( $\mu = a, b$ ), and  $\omega_k$  is the frequency of the  $k^{\text{th}}$  mode in the waveguide. In most of the numerical simulation we often take  $\omega_a = \omega_b = \omega$ . The operators  $\sigma_{\mu}^{+}$  and  $\sigma_{\mu}^{-}$  represent the raising and lowering operators, and  $c_k$  is the photon annihilation operator.

Equation (4) describes the interaction between two giant atoms and a waveguide in frequency domain. From the perspective of spatial distribution, the coupling between atoms and the waveguide can be characterized by a spatial distribution function  $g_{\mu}(x)$ . The frequency-dependent coupling strength  $G_{\mu k}$  is given by a Fourier transformation [77]

$$G_{\mu k} = \int dx g_{\mu}(x) e^{-ikx}. \quad (5)$$

In the limiting case that the size of the atoms is extremely small,  $g_{\mu}(x)$  is reduced to  $\delta$ -function as shown in Fig. 1(a), the model is reduced to the small atom case, since each atom only couples to the waveguide at a single point. In this case, the photon emission and absorption is the simplest. Photon emitted from one atom must be absorbed by the other one at the fixed position.

In most existing studies about giant atoms [2, 17–19, 32, 33], researchers mainly focus on the case that giant atoms are coupled to the waveguide with two or finite coupling points as shown in Fig. 1(b). In this case, photon emitted, for instance, at  $x_{a1}$  can be absorbed at different positions. But the choice is still limited. It is worth to note that the case of two coupling points is sufficient to capture most of the interesting physical phenomena arising from photon emission and absorption, although the photon emission and absorption are still simple. In this paper, we consider the most general case as shown in Fig. 1(c), the distribution function  $g_\mu(x)$  is a continuous distribution in the space domain. This enables more complicated photon emission and absorption process.

### III. LIMITATION OF THE CONVENTIONAL SINGLE-EXCITATION APPROACH

The most widely used method for solving the dynamics of giant atom systems is the dressed state method, in which the Hilbert space is often limited in single (or a few) excitation subspace [4, 13, 55, 78]. For example, in the model described in Eq. (1), the total excitation number operator  $N = \sum_{\mu=a,b} \sigma_\mu^+ \sigma_\mu^- + \sum_k c_k^\dagger c_k$  is a conserved quantity, then an arbitrary quantum state in the single-excitation subspace of the system can be expressed as

$$|\psi^{(1)}(t)\rangle = \sum_{\mu=a,b} A_\mu(t) e^{-i\omega_\mu t} \sigma_\mu^+ |G\rangle + \sum_k B_k(t) e^{-i\omega_k t} c_k^\dagger |G\rangle, \quad (6)$$

with  $\sum_{\mu=a,b} |A_\mu(t)|^2 + \sum_k |B_k(t)|^2 = 1$ , where  $|G\rangle = |g_a\rangle|g_b\rangle|0\rangle$  represents the waveguide is in the vacuum state and the giant atoms are in their ground states. The  $A_\mu(t)$  is the probability amplitude of the atom “ $\mu$ ”, and  $B_k(t)$  denotes the single-photon probability amplitude of the mode  $k$ . Based on the Schrödinger equation  $\frac{d}{dt}|\psi^{(1)}(t)\rangle = -iH_{\text{tot}}|\psi^{(1)}(t)\rangle$ , one can obtain the equations of motion for these probability amplitudes [55]

$$\begin{aligned} \dot{A}_\mu(t) &= -i \sum_k G_{\mu k}^* B_k(t) e^{-i(\omega_k - \omega_\mu)t}, \\ \dot{B}_k(t) &= -i \sum_{\mu=a,b} G_{\mu k} A_\mu(t) e^{i(\omega_k - \omega_\mu)t}. \end{aligned} \quad (7)$$

Subsequently, the system dynamics can be found by solving above differential equations.

However, the limitation of this method is obvious. When the excitation number is high, both the number and complexity of the equations will increase significantly (see Sec. VIA). Besides, the waveguide supports a continuum of modes, including those with vanishingly low frequencies ( $\omega_k \rightarrow 0$ ). Even near absolute zero, these low-frequency modes maintain a non-negligible thermal population  $\bar{n}_k = 1/(e^{\beta\hbar\omega_k} - 1)$ . Consequently, at any finite temperature ( $T > 0$ ), the waveguide is inherently

in a multi-excitation state. This invalidates the single-excitation assumption. Thus, the limitation of this conventional approach demands a new framework.

### IV. STOCHASTIC SCHRÖDINGER EQUATION APPROACH

#### A. Equation for the stochastic state vector

To overcome the limitations of the single-excitation approximation, we propose the SSE approach based on the non-Markovian quantum state diffusion approach [61–72]. Next, we start from the original Hamiltonian (1) to derive the SSE for the two giant atoms, as well as the master equation.

To focus on the dynamics of the giant atoms, the reduced density operator is defined by performing a partial trace over the waveguide degrees of freedom

$$\rho(t) = \text{tr}_W [|\psi_{\text{tot}}(t)\rangle\langle\psi_{\text{tot}}(t)|]. \quad (8)$$

Evaluating this trace in the Fock basis is the most intuitive approach, yielding

$$\rho(t) = \sum_{\{n_k\}} \langle\{n_k\}|\psi_{\text{tot}}(t)\rangle\langle\psi_{\text{tot}}(t)|\{n_k\}\rangle, \quad (9)$$

where  $|\{n_k\}\rangle \equiv \prod \otimes_k |n_k\rangle$  denotes the multi-mode Fock state of the waveguide, with each mode  $k$  in the Fock state  $|n_k\rangle$ . However, since the waveguide contains infinite modes, resulting in a prohibitively large Hilbert space, making this Fock-basis trace evaluation computationally intractable.

To overcome this difficulty, we transform the partial trace into a stochastic averaging problem by using the Bargmann coherent states  $|z\rangle \equiv \prod \otimes_k |z_k\rangle$ , with each mode  $k$  in the coherent state  $|z_k\rangle$ . The properties of coherent states (e.g.,  $c_k|z\rangle = z_k|z\rangle$ ) facilitate the subsequent derivation of the dynamical equation. Substituting the completeness relation  $\int \frac{d^2z}{\pi} e^{-|z|^2} |z\rangle\langle z| = 1$  into the trace operation in Eq. (9), the reduced density operator can be rewritten as

$$\begin{aligned} \rho(t) &= \int \frac{d^2z}{\pi} e^{-|z|^2} \langle z|\psi_{\text{tot}}(t)\rangle\langle\psi_{\text{tot}}(t)|z\rangle \\ &\equiv \mathcal{M}[|\psi(t, z^*)\rangle\langle\psi(t, z)|], \end{aligned} \quad (10)$$

where the stochastic state vector is defined as

$$|\psi(t, z^*)\rangle \equiv \langle z|\psi_{\text{tot}}(t)\rangle, \quad (11)$$

and the stochastic average is defined as  $\mathcal{M}[\cdot] \equiv \int \frac{d^2z}{\pi} e^{-|z|^2} [\cdot]$  [61, 63]. Equation (10) clarifies the physical meaning of the stochastic state vector  $|\psi(t, z^*)\rangle$ . For a particular set of parameters  $\{z_k\}$ ,  $|\psi(t, z^*)\rangle$  represents a possible trajectory. The statistical average over all possible trajectories will reproduce the density operator  $\rho(t)$  [61, 63].

Next, we will derive the equation governing the evolution of the stochastic state vector  $|\psi(t, z^*)\rangle$ . As we know, the total state vector  $|\psi_{\text{tot}}(t)\rangle$  satisfies the Schrödinger equation  $\frac{d}{dt}|\psi_{\text{tot}}(t)\rangle = -iH_{\text{tot}}^I(t)|\psi_{\text{tot}}(t)\rangle$ , where

$$H_{\text{tot}}^I(t) = H_A + \sum_{\mu=a,b} \left( \sum_k G_{\mu k} \sigma_{\mu}^- c_k^\dagger e^{i\omega_k t} + \text{H.c.} \right), \quad (12)$$

is the Hamiltonian in the interaction picture with respect to  $H_W$ . Taking time derivative to both sides of Eq. (11) and substituting the Schrödinger equation, one obtains

$$\begin{aligned} \frac{d}{dt}|\psi(t, z^*)\rangle = & \left[ -iH_A + \sum_{\mu=a,b} \left( \sigma_{\mu}^- z_{\mu t}^* \right. \right. \\ & \left. \left. - i\sigma_{\mu}^+ \sum_k G_{\mu k}^* e^{-i\omega_k t} \frac{\partial}{\partial z_k^*} \right) \right] |\psi(t, z^*)\rangle, \end{aligned} \quad (13)$$

where  $z_{\mu t}^* \equiv -i \sum_k G_{\mu k} z_k^* e^{i\omega_k t}$  is a  $z_k$ -dependent function. Given a particular set of  $z_k^*$ , there will be a realization of  $z_{\mu t}^*$  and a corresponding solution  $|\psi(t, z^*)\rangle$  of

Eq. (13). Diósi et al. [61] named  $z_{\mu t}^*$  as a stochastic noise and the corresponding solution  $|\psi(t, z^*)\rangle$  is called a quantum trajectory. In principle, the density operator can be retrieved by integrating over all possible trajectories as shown in Eq. (10). However, in practical scenarios, there is no need to generate an infinite number of trajectories. Only a few hundred (at most a few thousand) randomly generated trajectories are enough to reproduce density operator with high precision. This approach replaces the cumbersome trace operation in Eq. (8) with a stochastic average over trajectories, thereby greatly simplifying the computation.

Equation (13) is merely a formal dynamical equation. It contains both  $z_{\mu t}^*$  and  $\frac{\partial}{\partial z_k^*}$ . To obtain a computationally tractable equation which only depends on  $z_{\mu t}^*$  and the time  $t$ , one can use the chain rule to replace the term  $\frac{\partial}{\partial z_k^*}|\psi(t, z^*)\rangle$  by a functional derivative  $-i \sum_k G_{\mu k} \sigma_{\mu}^+ e^{-i\omega_k t} \frac{\partial}{\partial z_k^*} = -\sigma_{\mu}^+ \int_0^t ds [\sum_k \frac{\partial z_{\mu t}}{\partial z_k} (\frac{\partial z_{\mu s}^*}{\partial z_k^*} \frac{\delta}{\delta z_{\mu s}^*} + \frac{\partial z_{\nu s}^*}{\partial z_k^*} \frac{\delta}{\delta z_{\nu s}^*})]$  ( $\mu, \nu = a, b; \mu \neq \nu$ ). Then, Eq. (13) becomes

$$\frac{d}{dt}|\psi(t, z^*)\rangle = \sum_{\substack{\mu, \nu=a,b \\ \mu \neq \nu}} \left\{ -iH_A + \sigma_{\mu}^- z_{\mu t}^* - \sigma_{\mu}^+ \int_0^t ds \left[ \alpha_{\mu\mu}(t, s) \frac{\delta}{\delta z_{\mu s}^*} + \alpha_{\mu\nu}(t, s) \frac{\delta}{\delta z_{\nu s}^*} \right] \right\} |\psi(t, z^*)\rangle. \quad (14)$$

where

$$\alpha_{\mu\mu}(t, s) = \sum_k \frac{\partial z_{\mu t}}{\partial z_k} \frac{\partial z_{\mu s}^*}{\partial z_k^*} = \sum_k |G_{\mu k}|^2 e^{-i\omega_k(t-s)}, \quad (15)$$

are the auto-correlation functions, and

$$\alpha_{\mu\nu}(t, s) = \sum_k \frac{\partial z_{\mu t}}{\partial z_k} \frac{\partial z_{\nu s}^*}{\partial z_k^*} = \sum_k G_{\mu k}^* G_{\nu k} e^{-i\omega_k(t-s)}, \quad (16)$$

are the cross-correlation functions for subscripts  $\mu \neq \nu$ . Equation (14) is directly derived from Schrödinger equation and includes stochastic noises  $z_{\mu t}^*$ , thus it is called the SSE [61–63].

It is important to note that the correlation functions  $\alpha_{\mu\mu}$  and  $\alpha_{\mu\nu}$  encode all information about the interactions between giant atoms and waveguide. We emphasize that these functions are predetermined by the physical setup described by the spatial coupling distribution  $g_{\mu}(x)$ . They are independent of the state of the giant atoms. Actually, the correlation functions can also be defined in terms of the interaction Hamiltonian, which is presented in Appendix A. This confirms from another perspective that the coupling between the waveguide and the giant atoms can be encoded in the correlation functions. It is straightforward to check the correlation functions characterize the statistics of noise  $z_{\mu t}^*$ , as evidenced

by the following relations

$$\begin{aligned} \mathcal{M}[z_{\mu t}] &= \mathcal{M}[z_{\mu t} z_{\mu s}] = 0, \\ \mathcal{M}[z_{\mu t} z_{\mu s}^*] &= \alpha_{\mu\mu}(t, s), \quad \mathcal{M}[z_{\mu t} z_{\nu s}^*] = \alpha_{\mu\nu}(t, s). \end{aligned} \quad (17)$$

In the numerical simulation, one need to generate stochastic functions  $z_{\mu t}^*$  that satisfies these correlation functions [71]. The detailed discussion about the correlation functions is presented in Sec. V.

Up to this point, we have derived SSE in Eq. (14). Starting from nothing more than the Hamiltonian, we expand the state vector  $|\psi_{\text{tot}}\rangle$  into many stochastic state vectors  $|\psi(t, z^*)\rangle$  using the coherent state basis and derived corresponding equation governing the dynamics of  $|\psi(t, z^*)\rangle$  (SSE). Solving the SSE under different noise realizations  $z_{\mu t}^*$  produces numerous dis-

tinct trajectories  $|\psi(t, z^*)\rangle$ . Averaging these trajectories as  $\mathcal{M}[|\psi(t, z^*)\rangle\langle\psi(t, z)|]$  yields the density operator  $\rho(t)$ . Throughout the derivation, we only employ the Schrödinger equation, thus the SSE is purely a mathematical result.

Besides, our Hamiltonian contains two different coupling  $G_{\mu k}$ , thus we introduce two noises  $z_{\mu t}^*$  ( $\mu = a, b$ ), resulting in two types of correlation functions, auto- and cross-correlation functions. This is an extension of the original SSE approach [61–63]. In our study of giant atoms, a by-product emerged, that the framework of the SSE approach is extended to the case involving two types of noises and correlation functions.

## B. Mathematical Techniques for solving SSE

The primary challenge in solving Eq. (14) stems from the functional derivatives  $\frac{\delta}{\delta z_{\mu s}^*}|\psi(t, z^*)\rangle$ . To address this difficulty, we introduce time-dependent operators  $O_\mu$  ( $\mu = a, b$ ) defined as

$$\frac{\delta}{\delta z_{\mu s}^*}|\psi(t, z^*)\rangle = O_\mu(t, s, z^*)|\psi(t, z^*)\rangle. \quad (18)$$

With the operators  $O_\mu$ , Eq. (14) is rewritten as

$$\begin{aligned} \frac{d}{dt}|\psi(t, z^*)\rangle &= H_{\text{eff}}|\psi(t, z^*)\rangle \\ H_{\text{eff}} &= -iH_A + \sum_{\mu=a,b} [\sigma_\mu^- z_{\mu t}^* - \sigma_\mu^+ \bar{O}_\mu(t, z^*)] \end{aligned} \quad (19)$$

$$\frac{\partial}{\partial t} \frac{\delta}{\delta z_{\mu s}^*}|\psi(t, z^*)\rangle = \left( \frac{\partial}{\partial t} O_\mu \right) |\psi(t, z^*)\rangle + O_\mu \frac{\partial}{\partial t} |\psi(t, z^*)\rangle = \left( \frac{\partial}{\partial t} O_\mu + O_\mu H_{\text{eff}} \right) |\psi(t, z^*)\rangle, \quad (22)$$

and the right-hand-side (RHS) yields

$$\frac{\delta}{\delta z_{\mu s}^*} \frac{\partial}{\partial t} |\psi(t, z^*)\rangle = \left( \frac{\delta}{\delta z_{\mu s}^*} H_{\text{eff}} \right) |\psi(t, z^*)\rangle + H_{\text{eff}} \left( \frac{\delta}{\delta z_{\mu s}^*} |\psi(t, z^*)\rangle \right) = \left( H_{\text{eff}} O_\mu - \sum_{\nu=a,b} \sigma_\nu^+ \frac{\delta}{\delta z_{\mu s}^*} \bar{O}_\nu \right) |\psi(t, z^*)\rangle. \quad (23)$$

Equating LHS and RHS, one can obtain

$$\frac{\partial}{\partial t} O_\mu = \sum_{\nu=a,b} \left\{ [-iH_A + \sigma_\nu^- z_{\nu t}^* - \sigma_\nu^+ \bar{O}_\nu, O_\mu] - \sigma_\nu^+ \frac{\delta}{\delta z_{\mu s}^*} \bar{O}_\nu \right\}, \quad (24)$$

subject to the initial conditions  $O_\mu(t, s = t, z^*) = \sigma_\mu^-$ . In this model, it is straightforward to obtain the solution for  $O_\mu$  is [67]

$$O_\mu(t, s) = \sum_{j=1}^4 p_{\mu j}(t, s) O_{\mu j}, \quad (25)$$

where the operators  $\bar{O}_\mu$  are defined as

$$\bar{O}_\mu(t, z^*) = \int_0^t ds \sum_{\nu=a,b} [\alpha_{\mu\nu}(t, s) O_\nu(t, s, z^*)]. \quad (20)$$

For simplicity, we use the abbreviations  $O_\mu \equiv O_\mu(t, s, z^*)$  and  $\bar{O}_\mu \equiv \bar{O}_\mu(t, z^*)$  if no confusion arises.

Now, if the solution of  $O_\mu$  can be found, Eq. (14) can be solved as an ordinary differential equation with stochastic variables. Actually, the operators  $O_\mu$  can be determined through the consistency condition [63]

$$\frac{\partial}{\partial t} \frac{\delta}{\delta z_{\mu s}^*}|\psi(t, z^*)\rangle = \frac{\delta}{\delta z_{\mu s}^*} \frac{\partial}{\partial t} |\psi(t, z^*)\rangle. \quad (21)$$

Substituting Eq. (19) into Eq. (21), the left-hand-side (LHS) yields

$$\frac{\partial}{\partial t} \frac{\delta}{\delta z_{\mu s}^*}|\psi(t, z^*)\rangle = \left( \frac{\partial}{\partial t} O_\mu \right) |\psi(t, z^*)\rangle + O_\mu \frac{\partial}{\partial t} |\psi(t, z^*)\rangle = \left( \frac{\partial}{\partial t} O_\mu + O_\mu H_{\text{eff}} \right) |\psi(t, z^*)\rangle, \quad (22)$$

where the basis operators are

$$\begin{aligned} O_{\mu 1} &= \sigma_\mu^-, \quad O_{\mu 2} = \sigma_\mu^z \sigma_\nu^-, \\ O_{\mu 3} &= \sigma_\nu^-, \quad O_{\mu 4} = \sigma_\nu^z \sigma_\mu^-. \end{aligned} \quad (26)$$

According to Eq. (24), the time-dependent coefficients  $p_{\mu j}$  are governed by the coupled partial differential equations

$$\begin{aligned}
\frac{\partial p_{\mu 1}}{\partial t} = & i\omega_\mu p_{\mu 1} + p_{\mu 1} P_{\mu 1} + p_{\mu 1} Q_{\nu 3} + p_{\mu 1} Q_{\mu 2} + p_{\mu 1} P_{\nu 4} - p_{\mu 2} Q_{\mu 1} + p_{\mu 2} Q_{\mu 4} \\
& + p_{\mu 2} P_{\nu 2} - p_{\mu 2} P_{\nu 3} + p_{\mu 4} P_{\mu 4} + p_{\mu 4} Q_{\nu 2} + p_{\mu 4} Q_{\mu 2} + p_{\mu 4} P_{\nu 4}, \\
\frac{\partial p_{\mu 2}}{\partial t} = & i\omega_\nu p_{\mu 2} + p_{\mu 2} P_{\mu 4} + p_{\mu 2} Q_{\nu 2} + p_{\mu 2} Q_{\mu 3} + p_{\mu 2} P_{\nu 1} + p_{\mu 1} P_{\mu 2} - p_{\mu 1} P_{\mu 3} \\
& - p_{\mu 1} Q_{\nu 1} + p_{\mu 1} Q_{\nu 4} + p_{\mu 3} P_{\mu 4} + p_{\mu 3} Q_{\nu 2} + p_{\mu 3} Q_{\mu 2} + p_{\mu 3} P_{\nu 4}, \\
\frac{\partial p_{\mu 3}}{\partial t} = & i\omega_\nu p_{\mu 3} + p_{\mu 3} P_{\nu 1} + p_{\mu 3} Q_{\mu 3} + p_{\mu 3} Q_{\nu 2} + p_{\mu 3} P_{\mu 4} - p_{\mu 4} Q_{\nu 1} + p_{\mu 4} Q_{\nu 4} \\
& + p_{\mu 4} P_{\mu 2} - p_{\mu 4} P_{\mu 3} + p_{\mu 2} P_{\mu 4} + p_{\mu 2} Q_{\nu 2} + p_{\mu 2} Q_{\mu 2} + p_{\mu 2} P_{\nu 4}, \\
\frac{\partial p_{\mu 4}}{\partial t} = & i\omega_\mu p_{\mu 4} + p_{\mu 4} P_{\mu 1} + p_{\mu 4} Q_{\nu 3} + p_{\mu 4} Q_{\mu 2} + p_{\mu 4} P_{\nu 4} + p_{\mu 1} P_{\mu 4} + p_{\mu 1} Q_{\nu 2} \\
& + p_{\mu 1} Q_{\mu 2} + p_{\mu 1} P_{\nu 4} - p_{\mu 3} Q_{\mu 1} + p_{\mu 3} Q_{\mu 4} + p_{\mu 3} P_{\nu 2} - p_{\mu 3} P_{\nu 3},
\end{aligned} \tag{27}$$

with the initial conditions

$$p_{\mu 1}(t, s=t) = 1, \quad p_{\mu j}(t, s=t) = 0 \quad (j \neq 1). \tag{28}$$

The coefficients  $P_{\mu j}$  and  $Q_{\mu j}$  are defined as  $P_{\mu j}(t) = \int_0^t ds \alpha_{\mu\mu}(t, s) p_{\mu j}(t, s)$  and  $Q_{\mu j}(t) = \int_0^t ds \alpha_{\nu\mu}(t, s) p_{\mu j}(t, s)$  with  $j = 1, 2, 3, 4$ . It is clear that  $P_{\mu j}$  and  $Q_{\mu j}$  are time domain convolutions for auto- and cross-correlation functions, representing the cumulative effect of the impacts exerted by all past moments  $s$  on the present moment  $t$ .

### C. Derivation of master equation from SSE

With the solution in Eq. (25), Eq. (19) can be solved numerically. However, to further obtain the density operator  $\rho(t)$ , one needs to solve Eq. (19) repeatedly and obtain a large amount of trajectories of  $|\psi(t, z^*)\rangle$  with different noise realizations  $z_{\mu t}^*$ . The density operator  $\rho$  is then obtained by taking the statistical average over these trajectories, as shown in Eq. (10).

Alternatively, one may also derive the master equation based on Eq. (19). Following the method established in [79, 80], the master equation can be derived as (see Appendix B for details)

$$\frac{d}{dt} \rho = -i[H_A, \rho] + \sum_{\mu=a,b} ([\sigma_\mu^-, \rho \bar{O}_\mu^\dagger] + \text{H.c.}). \tag{29}$$

Notably, when the correlation functions  $\alpha_{\mu\nu}(t, s)$  ( $\mu, \nu = a, b$ ) is reduced to delta-functions  $\alpha_{\mu\nu}(t, s) = \Gamma \delta(t, s)$ , it is straightforward to check all the coefficients  $P$  and  $Q$  are all zero except  $P_{\mu 1} = \Gamma/2$  and  $Q_{\mu 1} = \Gamma/2$ . Thus,  $\bar{O}_\mu = \Gamma/2(\sigma_\mu^- + \sigma_\nu^+)$  and the master equation is reduced to the Lindblad master equation commonly used in the references [4, 18]

$$\frac{d}{dt} \rho = -i[H_A, \rho] + \sum_{\substack{\mu, \nu=a,b \\ \mu \neq \nu}} \frac{\Gamma}{2} \{ [\sigma_\mu^-, \rho(\sigma_\mu^+ + \sigma_\nu^+)] + \text{H.c.} \}. \tag{30}$$

This limiting case provides an important connection to conventional quantum optical treatment.

## V. ENTANGLEMENT DYNAMICS WITH CONTINUOUS COUPLING

Based on the SSE approach presented in Sec. IV, we will investigate entanglement between two giant atoms from another perspective and reveal the physical meaning of the correlation functions, which is rarely touched in existing literature. Throughout our analysis, we quantify entanglement by using the well-established entanglement measure, “concurrence”  $C$  [81].

### A. Transition from discrete coupling to continuous coupling

We start from a comb-like discrete coupling distribution. The comb-like distribution function is defined as

$$g_\mu(x) = \frac{1}{\tilde{N}} \sum_{i=1}^m \delta(x - x_{\mu i}), \quad (\mu = a, b) \tag{31}$$

where  $\tilde{N}$  denotes the normalization factor, while  $x_{\mu i}$  corresponds to the spatial coordinates of non-zero coupling points,  $m$  represents the number of coupling points. Such a distribution describes the giant atoms are coupled to waveguide only at several discrete points  $x = x_{\mu i}$ , illustrated in Fig. 2(a)-(c). The distance is measured in units of the wavelength  $\lambda = c/\omega$ , where  $c$  is the speed of light (setting to be 1) and  $\omega = \omega_a = \omega_b$  is the transition frequency of two atoms (setting to be identical). Similarly, time is scaled by the dimensionless quantity  $\omega\tau$ . All the figures throughout the paper are presented in this set of dimensionless units.

Before investigating the time evolution of the quantum states, we first explore how correlation functions vary with the number of coupling points. The corresponding correlation functions for each distribution are displayed in Fig. 2(d)-(f). As shown in Eq. (15) and Eq. (16), the correlation functions are independent of the initial state and is determined solely by the distribution of coupling.

For single coupling point ( $m = 1$ ) in Fig. 2(a) and (d), the cross-correlation function, for example  $\alpha_{ab}(\tau)$ , ex-

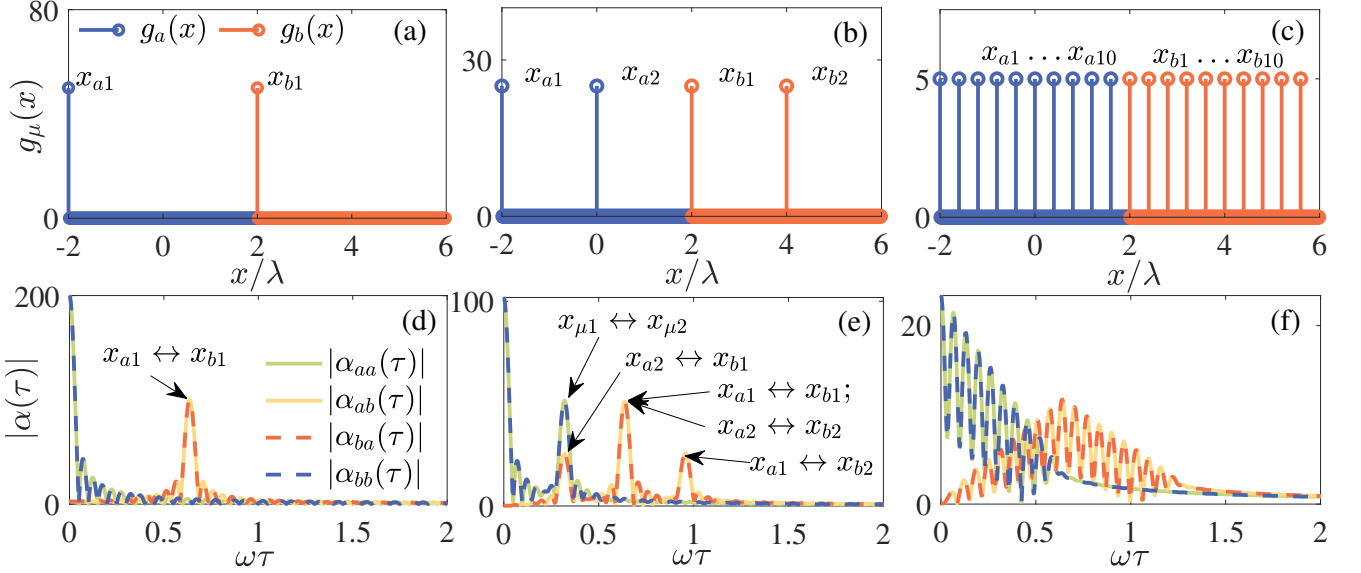


FIG. 2. (a)-(c) Discrete coupling distributions for  $m = 1$ ,  $m = 2$ , and  $m = 10$  coupling points, respectively. (d)-(f) Auto- and cross-correlation functions for  $m = 1$ ,  $m = 2$ , and  $m = 10$ , respectively.

hibits a peak in the time domain. This indicates that only event (e.g., photon emitted at  $x_a$ ) occurring at a specific moment  $s = t - \tau$  in the past can exert an influence on the present event (e.g., photon absorbed at  $x_b$ ) at time  $t$ , and this particular moment precisely corresponds to the time required for a photon to propagate from point  $x_a$  to point  $x_b$ .

For two coupling points ( $m = 2$ ), the auto-correlation function  $\alpha_{\mu\mu}(\tau)$  in subplot (e) has one peak (except the one at  $\tau = 0$ ) that corresponds to the physical process that photon emitted at  $x_{\mu 1}$  (or  $x_{\mu 2}$ ) is absorbed at  $x_{\mu 2}$  (or  $x_{\mu 1}$ ). This allows a time delayed self-absorption at another coupling point for the same giant atom, which does not exist in the case of small atom. Besides, the cross-correlation function  $\alpha_{\mu\nu}(\tau)$  exhibits three peaks corresponding to three possible emission and absorption routes:  $x_{a2} \leftrightarrow x_{b1}$ ,  $x_{a1} \leftrightarrow x_{b1}$  ( $x_{a2} \leftrightarrow x_{b2}$ ), and  $x_{a1} \rightarrow x_{b2}$ , which have been marked in Fig. 2(e).

Extending to more coupling points ( $m = 10$ ) shown in Fig. 2(c) and (f), there are more feasible pathways for photon emission and absorption, which collectively constitute a highly sophisticated emission-absorption network. In Fig. 2(f), both the auto- and cross-correlation functions exhibit multiple peaks, which reflects that there exist more possibilities in the time duration for photons to undergo emission and absorption.

As can be seen from Fig. 2, within the framework of the SSE approach, the auto- and cross-correlation functions can, to some extent, reveal the impact of the delay effect on system dynamics. Notably, the calculation of the correlation functions depends solely on the distribution and strengths of coupling points. Consequently, we can gain preliminary insight into the role of the delay effect in dynamical evolution by solely considering the distri-

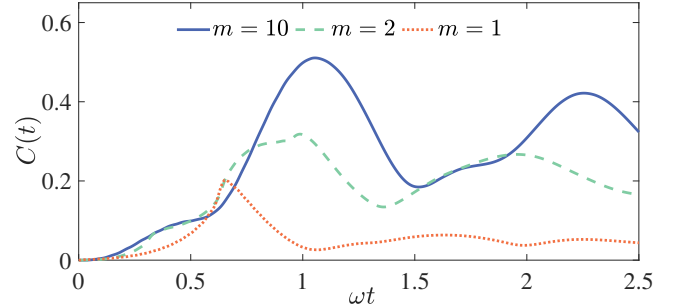


FIG. 3. Time evolution of concurrence  $C(t)$  for single-point (orange dotted), two-point (green dashed), and multi-point (blue solid) coupling cases. The parameters are identical to those in Fig. 2.

bution pattern and coupling strengths. This is a feature not possessed by conventional methods in Sec. III.

Having established that the correlation functions reflect the paths of photon emission and absorption, we next investigate how the number of coupling points influences the entanglement between the giant atoms. By choosing the initial state as  $|eg\rangle$ , the time evolution of the concurrence is plotted in Fig. 3. In the case of a single coupling point ( $m = 1$ , orange dotted line in Fig. 3), the generation of entanglement is transient and weak ( $C_{\max} \approx 0.2$ ), owing to the limited interaction pathways. When the number of coupling points is increased (e.g.,  $m = 2$  in Fig. 3) leads to a greater diversity of pathways for photon emission and absorption. Such multi-path interference results in enhanced entanglement generation, yielding a maximum entanglement of  $C_{\max} \approx 0.3$ . As the number of coupling points continues to increase ( $m = 10$

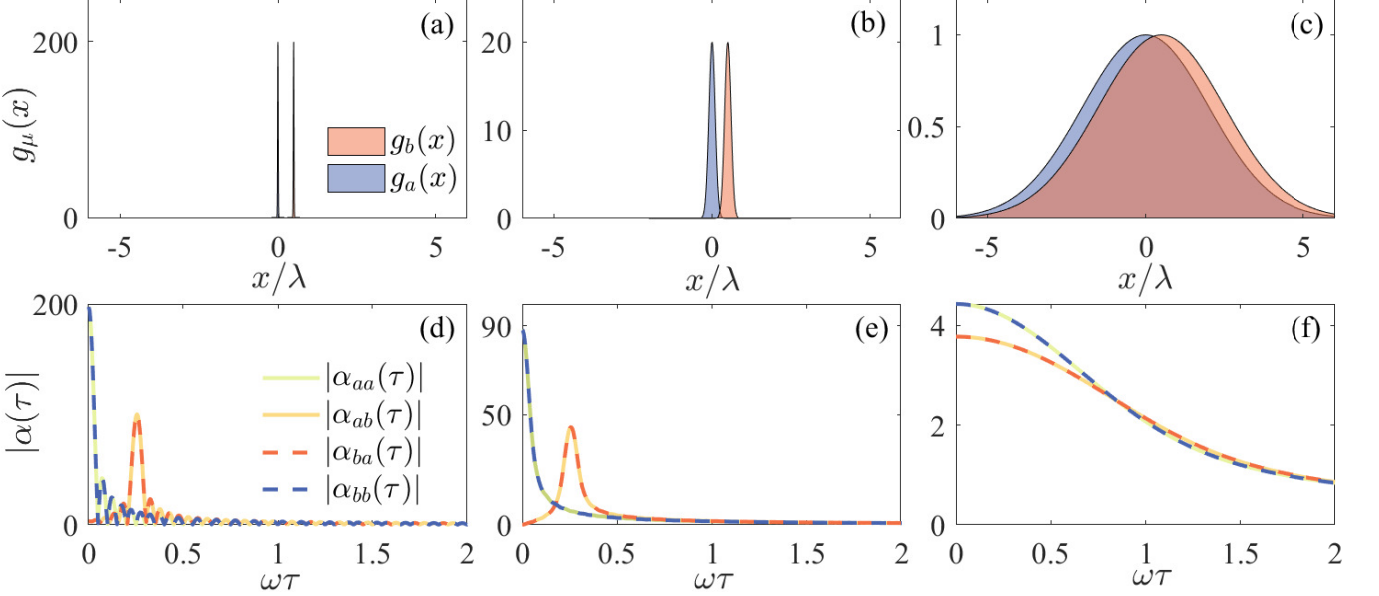


FIG. 4. Gaussian distribution  $g_\mu(x)$  for  $s_\mu = 0.01, 0.1$ , and  $2$  (assuming  $s_a = s_b$ ) are plotted in panels (a), (b), (c). The correlation functions  $\alpha_{\mu\nu}(\tau)$  for  $s_\mu = 0.01, 0.1$ , and  $2$  (assuming  $s_a = s_b$ ) are plotted in panels (d), (e), (f).

in Fig. 3), the peak value of entanglement  $C(t)$  increases significantly to  $0.5$  with a stronger revival. This behavior demonstrates that the multiple coherent feedback channels within the waveguide enable stronger and robust entanglement generation.

### B. Continuous coupling with Gaussian distribution

When the coupling points become sufficiently dense, the discrete distribution transitions into a continuous distribution. We assume the spatially dependent coupling distribution  $g_\mu(x)$  is a Gaussian distribution,

$$g_\mu(x) = \frac{1}{s_\mu \sqrt{2\pi}} \exp \left[ -\frac{(x - \bar{x}_\mu)^2}{2s_\mu^2} \right], \quad (\mu = a, b) \quad (32)$$

where  $\bar{x}_\mu$  denote the central positions and  $s_\mu$  characterize the distribution widths. The influence of the distribution width  $s_\mu$  is presented in Fig. 4. One may compare the results in Fig. 4 with those in Fig. 2. In the case of continuous coupling [except the extreme localization case depicted in Fig. 4(a)], the correlation functions in Fig. 4(e) and Fig. 4(f) evolve into continuous functions instead of exhibiting distinct peaks. This implies that events occurring at any arbitrary past time  $s$  can exert an influence on the current time  $t$ , rather than only those events at specific past times  $s$  (satisfying  $t - s = \tau_{peak}$ ) as observed

in Fig. 2. The fundamental reason is that in the case of continuous coupling, photons can be emitted from any coupling points and subsequently absorbed at any other coupling points, such that the propagation time involved can take on any arbitrary value. In contrast, under discrete coupling, photons can only be emitted and absorbed between a limited set of specific coupling points, which restricts their propagation time to a discrete set of values.

Further discussions on the effects of continuous coupling on entanglement generation, particularly the impact of the central positions  $\bar{x}_\mu$  of the continuous coupling, are discussed in Appendix C and Appendix D. We now proceed to present the most important results of this work.

### C. Breaking constant phase difference via continuous coupling

As mentioned in Sec. I, all intriguing phenomena in giant-atom systems stem from interference effects associated with photon emission and absorption processes. However, continuous coupling may break the constant phase difference condition, which consequently weaken such interference effects, as illustrated in Fig. 1(c). To show how continuous coupling impact interference effects, we consider the spatial distribution of the continuous coupling  $g_\mu(x)$  as a double-peak function

$$g_\mu(x) = \frac{1}{s_\mu \sqrt{2\pi}} \left\{ \exp \left[ -\frac{(x - \bar{x}_{\mu 1})^2}{2s_\mu^2} \right] + \exp \left[ -\frac{(x - \bar{x}_{\mu 2})^2}{2s_\mu^2} \right] \right\}. \quad (\mu = a, b) \quad (33)$$

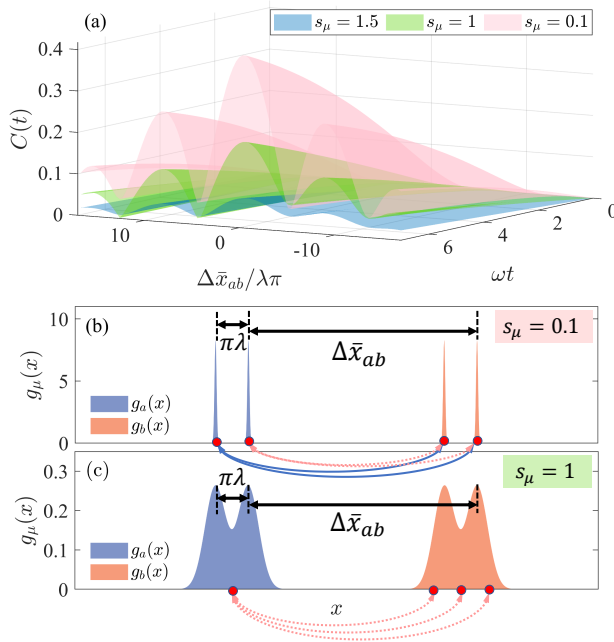


FIG. 5. The weakening of interference effects as a consequence of the broadening of the continuous coupling. (a) Entanglement generation for different spatial distributions of the continuous coupling  $g_\mu(x)$  given in Eq. (33). (b) and (c) are the distribution functions  $g_a(x)$  and  $g_b(x)$  for the case  $s_\mu = 0.1$  and  $s_\mu = 1$  (assuming  $s_a = s_b$ ), respectively.

This choice is motivated by the connection of this double-peak spatial distribution to the widely studied discrete coupling model with two coupling points [see Fig. 1(b)]. When the distribution width  $s_\mu \rightarrow 0$ , the double-peak distribution in Eq. (33) reduces to the well-established two-coupling-point configuration in Fig. 1(b). The interference phenomena have been extensively investigated in previous studies [40, 54, 55]. Varying  $s_\mu$  enables systematic exploration of how continuous coupling broadening modulates interference effects.

As shown in Fig. 5(b) and (c), each giant atom couples to the waveguide in two spatially separated regions centered at  $\bar{x}_{\mu 1}$  and  $\bar{x}_{\mu 2}$ . For both giant atoms, we now fix the inter-peak distance of  $g_\mu(x)$  as  $\bar{x}_{a2} - \bar{x}_{a1} = \bar{x}_{b2} - \bar{x}_{b1} = \pi\lambda$ . Then, the only crucial parameter becomes the distance

$$\Delta\bar{x}_{ab} = \bar{x}_{b1} - \bar{x}_{a1} = \bar{x}_{b2} - \bar{x}_{a2}, \quad (34)$$

which describes spatial separation between the centers of the relevant coupling regions corresponding to the two giant atoms “a” and “b” [see Fig. 5(b) and (c)]. The parameter  $\Delta\bar{x}_{ab}$  determines the phase accumulated when a photon travels from one giant atom to the other one. In the strongly-localized distribution case  $s_\mu = 0.1$ , as shown in Fig. 5(b), there is a strong interference because the phase difference accumulated is almost a constant. This is reflected in the entanglement generation shown in Fig. 5(a). The pink surface (for  $s_\mu = 0.1$ ) exhibits a

pattern analogous to interference fringes when  $\Delta\bar{x}_{ab}$  is varied.

In contrast, as  $s_\mu$  increases [e.g.,  $s_\mu = 1$  in Fig. 5(c)], the double-peak distribution of  $g_\mu(x)$  broadens significantly. Each giant atom couples to the waveguide in a much broader region. As illustrated in Fig. 5(c), there are many possible pathways for the photon to be emitted and absorbed by the two giant atoms, as a result, the phase accumulated by a photon traveling between the two atoms is no longer nearly constant. The breaking of constant phase different condition eventually weakens the interference pattern as shown in the green surface in Fig. 5(a).

When  $s_\mu$  is further increased to  $s_\mu = 1.5$ , the corresponding blue surface in Fig. 5(a) appears nearly flat, with only faint variations in entanglement generation. The periodic interference pattern has been erased by the broadened continuous coupling. This trend confirms that the broadening of continuous coupling directly suppresses the interference effects inherent to giant-atom systems.

## VI. MULTIPLE EXCITATIONS

In Sec. V, we mainly focus on the first gap that mentioned in Sec. V. In this section, we will try to fill the second gap and we extend the analysis beyond the single excitation subspace to investigate the dynamical properties within two- and multiple-excitations. We will start from the increased complexity of the conventional methods.

### A. Complexity of the conventional finite-excitation approach

The conventional dressed state approach has been reviewed in Sec. III. Now, we go beyond the single excitation subspace in Eq. (6) to assume two excitations. In the two-excitation subspace, the state vector can be expressed as

$$|\psi^{(2)}(t)\rangle = C_{ab}(t)\sigma_a^+\sigma_b^+|G\rangle + \sum_{\mu=a,b} \sum_k B_{\mu,k}(t)\sigma_\mu^+c_k^\dagger|G\rangle + \sum_{k \neq k'} A_{k,k'}(t)c_k^\dagger c_{k'}^\dagger|G\rangle, \quad (35)$$

Consequently, the dynamical equation. (7) must be reformulated into the following more intricate form,

$$\begin{aligned}\dot{C}_{ab}(t) &= -i \sum_{\mu=a,b} \sum_k G_{\mu k} e^{i(\omega_k - \omega_\mu)t} B_{\mu,k}(t), \\ \dot{B}_{\mu,k}(t) &= -i G_{\nu k}^* e^{-i(\omega_k - \omega_\nu)t} C_{ab}(t) \\ &\quad - i \sum_{k'} G_{\mu k} e^{i(\omega_{k'} - \omega_\mu)t} A_{k,k'}(t), \quad (\mu \neq \nu) \\ \dot{A}_{k,k'}(t) &= -i \sum_{\mu=a,b} G_{\mu k}^* e^{-i(\omega_k - \omega_\mu)t} B_{\mu,k'}(t) \\ &\quad - i \sum_{\mu=a,b} G_{\mu k'}^* e^{-i(\omega_{k'} - \omega_\mu)t} B_{\mu,k}(t),\end{aligned}\quad (36)$$

where  $C_{ab}(t)$  describes the double-atom excited state,  $B_{\mu,k}(t)$  ( $\mu = a, b$ ) describes the hybrid atom-waveguide excited states, and  $A_{k,k'}(t)$  corresponds to the double-waveguide excited state.

It is evident that employing the dressed state approach in the two-excitation regime leads to substantial complexity, posing significant challenges for both analytical derivation and numerical simulation. To consider more excitations, the complexity of analytical and numerical computation will be sharply increased. In contrast, the SSE approach in Sec. IV is independent of the specific form of the initial state as well as the total excitations. Compared to the single-excitation case, numerical simulations for two and more excitations only require a change of the initial state vector. Thus, the SSE approach demonstrates a clear advantage for addressing such problems and provides a valuable tool for research in this field.

### B. Double excitation state $|ee\rangle$

To demonstrate the advantage of the SSE approach, we begin with the entanglement generation process of a double excitation state  $|ee\rangle$  state. Here, we assume the single peak Gaussian distribution for the continuous coupling

$$g_\mu(x) = \frac{1}{s_\mu \sqrt{2\pi}} \exp \left[ -\frac{(x - \bar{x}_\mu)^2}{2s_\mu^2} \right]. \quad (\mu = a, b) \quad (37)$$

Comparing the numerical results in Fig. 6 and Fig. 7, we have two observations. First, the entanglement  $C(t)$  in the localized regime in Fig. 6 has a much stronger position dependent than the case in Fig. 7. The cross-section of entanglement  $C(t)$  in Fig. 6(b) is very sensitive to the distance  $\Delta\bar{x}_{ab} = \bar{x}_b - \bar{x}_a$ , while  $C(t)$  in Fig. 7(b) is insensitive to  $\Delta\bar{x}_{ab} = \bar{x}_b - \bar{x}_a$ . Second, the overall entanglement generation in the localized regime [Fig. 6(a)] is weaker than the delocalized regime [Fig. 7(a)]. This is reflected either from the maximum entanglement or from the average entanglement. The peak in Fig. 6(b) is less than 0.6, while the entanglement  $C(t)$  in Fig. 7(b) is always larger than 0.6 for any  $\Delta\bar{x}_{ab}$ , the peak is even larger than 0.8.

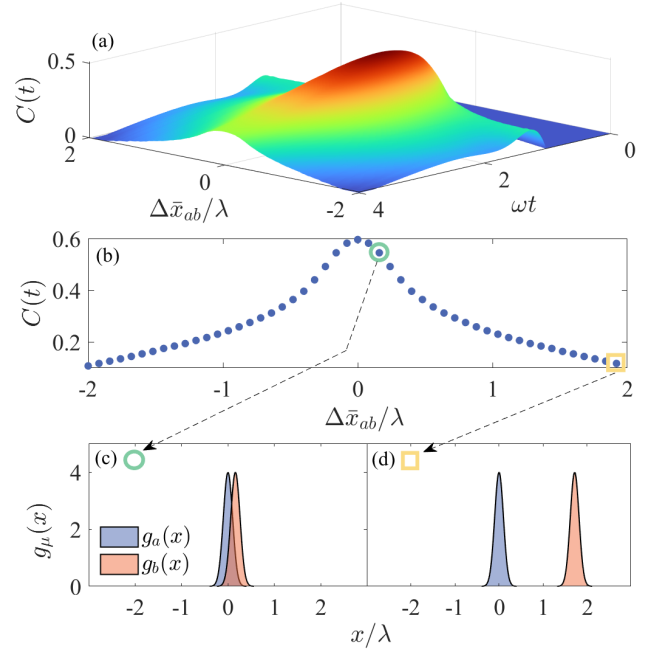


FIG. 6. Entanglement generation from the initial state  $|ee\rangle$  for strongly localized coupling ( $s_a = s_b = 0.1$ ). (a) 3D plot of concurrence  $C(t)$  versus time  $t$  and the distance between two centers of the coupling  $\Delta\bar{x}_{ab} = \bar{x}_b - \bar{x}_a$ . (b) 2D cross-section of  $C(t)$  at  $wt = 1.8$ . (c,d) Coupling distributions for: (c)  $\bar{x}_a = 0, \bar{x}_b = 0.16\lambda$ ; (d)  $\bar{x}_a = 0, \bar{x}_b = 1.92\lambda$ .

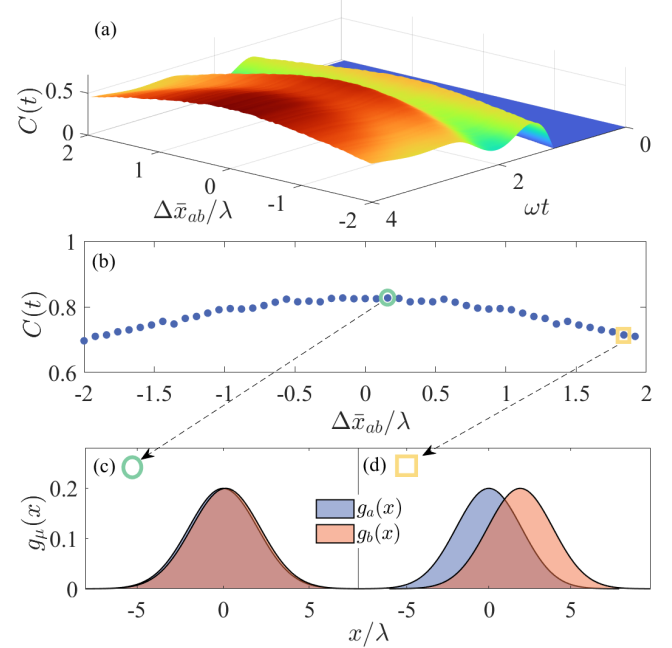


FIG. 7. Entanglement generation from the initial state  $|ee\rangle$  for strongly localized coupling ( $s_a = s_b = 2$ ). (a) 3D plot of concurrence  $C(t)$  versus time  $t$  and  $\Delta\bar{x}_{ab}$ . (b) 2D cross-section at  $wt = 1.8$  for  $C(t)$ . (c,d) Coupling distribution for: (c)  $\bar{x}_a = 0, \bar{x}_b = 0.16\lambda$ ; (d)  $\bar{x}_a = 0, \bar{x}_b = 1.92\lambda$ .

Both of the above two observations can be explained from the physical picture of photon emission and absorption. First, in the localized regime in Fig. 6, photons can be only emitted almost at a single point, and then absorbed also almost at a single point. The phase accumulation in the propagation process is close to a constant, which is sensitive to the distance  $\Delta\bar{x}_{ab} = \bar{x}_b - \bar{x}_a$ . Thus, a strong  $\Delta\bar{x}_{ab}$  dependence is observed in Fig. 6. As a comparison, in the delocalized regime in Fig. 7, photons can be emitted and absorbed at any points in the range of  $g_a(x)$  and  $g_b(x)$ . There are a large amount of trajectories corresponding to different phase accumulations. The influence of the distance  $\Delta\bar{x}_{ab}$  is smoothed out through averaging over all possible trajectories. Second, the delocalized distribution in Fig. 7 also provides more possibilities to build connections between two giant atoms through photon emission and absorption. Since there is not direct coupling between two giant atoms in the Hamiltonian (1), two giant atoms can be only indirectly coupled through the waveguide. More photon emission and absorption process means stronger indirect coupling, leading to stronger entanglement generation.

### C. Thermal and squeezed initial states of the waveguide

The SSE approach naturally extends to higher-excitation subspaces, providing a powerful tool to explore multi-photon initial state of the waveguide. For example, as we have discussed in Sec. I, the continuous spectrum of waveguide modes naturally involves the thermal initial state at finite temperatures. In Appendix E, we demonstrate that the SSE approach is compatible with thermal initial states. To be specific, one can introduce a set of fictitious modes with negative frequencies which has no interactions to both the giant atoms and the waveguide modes. By performing a Bogoliubov transformation, the thermal initial state of the waveguide is transformed into combined vacuum state for waveguide modes plus fictitious modes. Since the fictitious modes are isolated from other parts, it has no influence on the original dynamics. Thus, solving the model with the fictitious mode is equivalent to solving the original model with thermal initial states. The detailed derivation and discussion are presented in Appendix E.

The SSE approach also applicable to other nonclassical initial states, such as squeezed states (Appendix F). This enables the investigation of quantum dynamics in highly excited regimes and providing new perspectives on nonlinear quantum optical phenomena [60]. Although the detailed discussion can be left in a future study, we notice that the cross-correlation functions are enhanced [see Eq. (F6) and Eq. (F7)]. This implies the possibility of exponential enhancement [82–84] of cross-correlation function. From physical perspective, it means exponential enhancement of indirect interactions between two giant atoms. Therefore, our approach provide a theoret-

ical tool for the future study for enhanced interactions between giant atoms via squeezed states in waveguide.

Furthermore, this tool can be extended to investigate the role of the spatial structure of squeezing [85], which is anticipated to yield novel control over photon-mediated interactions in giant atom systems. This is also discussed in Appendix F.

## VII. CONCLUSION

This work establishes a systematic theoretical framework for investigating the dynamics of giant atoms coupled to a waveguide, which is applicable to continuous coupling and multiple-excitation scenarios and is further applied to study the entanglement dynamics of two giant atoms coupled to a single waveguide. To summarize, our work features the following key highlights.

(a) In the SSE approach, the auto- and cross-correlation functions offer a distinct perspective for quantifying the impact of time-delay effects.

(b) Continuous coupling yields distinct physical insights compared to the discrete coupling model widely studied in previous studies. Unlike discrete coupling where fixed optical paths enforce a constant phase difference, continuous coupling occurs over a spatial region, breaking the constant phase difference condition and thereby weakening interference-induced phenomena. This addresses Gap 1 identified in Sec. I.

(c) The SSE approach naturally handles multiple excitations. In traditional “dressed state approach”, the complexity of the dynamical equations increases drastically with the number of excitations. In contrast, in SSE approach, the dynamical equation remains unchanged as the number of excitations grows, greatly reducing the difficulty of numerical computations. Besides, we demonstrate that the SSE approach is compatible with both thermal and squeezed initial states, which opens a new window for future study on the introduction of squeezing in waveguides. This partially fills Gap 2 as mentioned in Sec. I.

(d) An additional contribution of this work is the incorporation of two types of noise calculations into the SSE framework, thereby extending the original SSE theoretical formalism [61–63].

We anticipate that the developed SSE framework will serve as a versatile platform for future investigations into the dynamics of giant atom-waveguide systems, particularly for exploring complex scenarios involving continuous coupling and multiple excitations.

## ACKNOWLEDGMENTS

We thank the support from the National Natural Science Foundation of China under Grant No. 62471143, the Key Program of National Natural Science Foundation of Fujian Province under Grant No. 2024J02008,

the project from Fuzhou University under Grant No. JG2020001-2, and the Natural Science Foundation of Fujian Province under Grant No. 2022J01548.

### Appendix A: Correlation function

There are two equivalent ways to define the correlation functions. The first one is presented in the main text, i.e.,

$$\alpha_{\mu\mu}(t, s) = \sum_k |G_{\mu k}|^2 e^{-i\omega_k(t-s)}. \quad (\text{A1})$$

In this definition,  $\alpha_{\mu\mu}$  (as an example, the other ones are similar) is interpreted as a Fourier transform of  $|G_{\mu k}|^2$ . The second definition is based on the collective coupling operator defined as  $C_\mu(t) \equiv \sum_k G_{\mu k} c_k^\dagger e^{i\omega_k t}$ . Given this operator, the interaction Hamiltonian can be written as

$$\begin{aligned} H_{\text{tot}}^I(t) &= H_A + \sum_{\mu=a,b} \left( \sum_k G_{\mu k} \sigma_\mu^- c_k^\dagger e^{i\omega_k t} + \text{H.c.} \right) \\ &= H_A + \sum_{\mu=a,b} (\sigma_\mu^- C_\mu^\dagger + \text{H.c.}) . \end{aligned} \quad (\text{A2})$$

Then, the correlation function can be expressed as the expectation value of operator  $C_\mu(t)C_\mu^\dagger(s)$  in the vacuum state, i.e.,

$$\alpha_{\mu\mu}(t, s) = \langle 0 | C_\mu(t) C_\mu^\dagger(s) | 0 \rangle. \quad (\text{A3})$$

One can check these two definition are equivalent [72]. The second definition reveals from another perspective that the correlation function reflects the nature of the coupling between the giant atoms and the waveguide.

### Appendix B: Master equation

The density operator can be reconstructed by averaging all the possible stochastic quantum trajectories as shown in Eq. (10). Define  $P_t \equiv |\psi(t, z^*)\rangle\langle\psi(t, z)|$  as the stochastic density operator, then take the time derivative of  $\rho = \mathcal{M}\{P_t\}$ , yielding

$$\begin{aligned} \frac{d}{dt}\rho &= \frac{d}{dt}\mathcal{M}\{P_t\} \\ &= \mathcal{M}\left\{ \left[ \frac{d}{dt}|\psi(t, z^*)\rangle \right] \langle\psi(t, z)| \right\} \\ &\quad + \mathcal{M}\left\{ |\psi(t, z^*)\rangle \left[ \frac{d}{dt}\langle\psi(t, z)| \right] \right\} \\ &= \mathcal{M}\{H_{\text{eff}}P_t\} + \mathcal{M}\{P_tH_{\text{eff}}\}. \end{aligned} \quad (\text{B1})$$

In the above equation, we employ the SSE in Eq. (19) to substitute  $\frac{d}{dt}|\psi(t, z^*)\rangle$  with  $H_{\text{eff}}|\psi(t, z^*)\rangle$ . It is straightforward to show that  $\mathcal{M}\{-iH_A P_t\} = -iH_A \mathcal{M}\{P_t\} = -iH_A \rho$ , since  $H_A$  is independent of the noise variables  $z$  or  $z^*$ . However, computing  $\mathcal{M}\{\sigma_\mu^- z_t^* P_t\}$  is no longer a trivial task. To evaluate this term, we will invoke the Novikov theorem as

$$\mathcal{M}\{P_t z_{\mu t}\} = \mathcal{M}\{\bar{O}_\mu P_t\}, \quad (\text{B2})$$

$$\mathcal{M}\{z_{\mu t}^* P_t\} = \mathcal{M}\{P_t \bar{O}_\mu^\dagger\}. \quad (\text{B3})$$

Here is a brief proof of the Novikov theorem, which is similar to the proof given in Refs. [63, 68]. By definition,

$$\begin{aligned} \mathcal{M}\{P_t z_{\mu t}\} &= \int \prod_k dz_k^* dz_k \exp\left(-\sum_k z_k^* z_k\right) P_t \left( i \sum_j G_j^* e^{-i\omega_j t} z_{\mu j} \right) \\ &= -i \sum_j G_j^* e^{-i\omega_j t} \int \prod_k dz_k^* dz_k P_t \frac{\partial}{\partial z_{\mu j}^*} \left[ \exp\left(-\sum_k z_k^* z_k\right) \right]. \end{aligned} \quad (\text{B4})$$

Integrating by parts and noting that in polar coordinates,  $[re^{-|r|^2}]_0^\infty = 0$ , one obtain

$$\begin{aligned} \mathcal{M}\{P_t z_{\mu t}\} &= i \sum_j G_{\mu j}^* e^{-i\omega_j t} z_{\mu j} \int \prod_k dz_k^* dz_k \frac{\partial}{\partial z_{\mu j}^*} P_t \exp\left(-\sum_k z_k^* z_k\right) \\ &= i \sum_j G_{\mu j}^* e^{-i\omega_j t} z_{\mu j} \int \prod_k dz_k^* dz_k \left( \int ds \frac{\partial z_{\mu s}^*}{\partial z_{\mu j}^*} \frac{\delta}{\delta z_{\mu s}^*} \right) P_t \exp\left(-\sum_k z_k^* z_k\right) \\ &= \int ds \sum_j |G_{\mu j}|^2 e^{-i\omega_j(t-s)} \int \prod_k dz_k^* dz_k \exp\left(-\sum_k z_k^* z_k\right) \frac{\delta}{\delta z_{\mu s}^*} P_t \\ &= \mathcal{M}\{\bar{O}_\mu P_t\}. \end{aligned} \quad (\text{B5})$$

Similarly, we can also prove

$$\mathcal{M}\{z_{\mu t}^* P_t\} = \mathcal{M}\{P_t \bar{O}_\mu^\dagger\}. \quad (\text{B6})$$

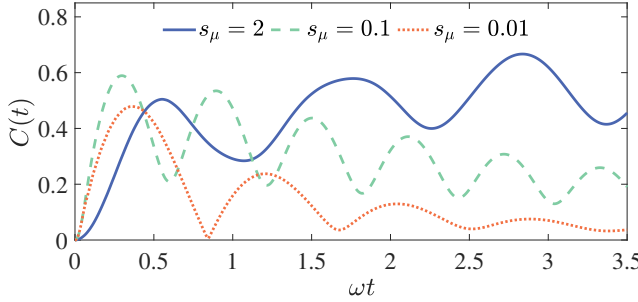


FIG. 8. Concurrence  $C(t)$  for different Gaussian coupling distributions  $s_\mu = 0.01$  (orange dotted),  $s_\mu = 0.1$  (green dashed), and  $s_\mu = 2$  (blue solid).

Applying the Novikov theorem (Eqs. B2 and B3) to Eq. B1, we arrive at the final master equation as

$$\frac{\partial}{\partial t}\rho = -i[H_A, \rho] + \sum_{\mu=a,b} ([\sigma_\mu^-, \mathcal{M}[P_t \bar{O}_\mu^\dagger]] + \text{H.c.}). \quad (\text{B7})$$

If  $O_\mu$  operator is independent of noise variable  $z$ , the master equation will reduce to

$$\frac{\partial}{\partial t}\rho = -i[H_A, \rho] + \sum_{\mu=a,b} ([\sigma_\mu^-, \rho \bar{O}_\mu^\dagger] + \text{H.c.}). \quad (\text{B8})$$

This is the master equation presented in Eq. (29) in the main text.

In Eq. (25), the solution of  $O_\mu$  operator is an approximate solution. The exact solution of  $O_\mu$  contains five terms with the fifth term associated with the operator  $O_{\mu 5} = \sigma_\mu^- \sigma_\nu^-$  to be  $z_{\mu t}^*$ -dependent [67]. Here, we take the noise free  $O$  operator  $O_\mu^{(0)}(t, s) = \sum_{j=1}^4 p_{\mu j}(t, s) O_{\mu j}$  as an approximate solution for computational efficiency, the calculation will be hugely reduced, since  $\mathcal{M}[P_t \bar{O}_\mu^\dagger] = \rho \bar{O}_\mu^\dagger$ . Meanwhile, the accuracy of this approximation is remarkable in many cases [86]. In Ref. [86], the authors show that the correction from the fifth term generally contributes only to fourth-order (or higher) effects in the coupling strengths. When  $G_{\mu k}$  is smaller than  $\omega_\mu$ , the noise term becomes negligible. Certainly, if necessary, one can derive the exact solution by following Ref. [67] in a straightforward manor. If the noise-dependent term  $O_{\mu 5}$  is taken into consideration, one can still derive a master equation by following the procedure in Ref. [80].

### Appendix C: Entanglement generation for continuous coupling with Gaussian distribution

In Sec. V B, we analyzed the continuous coupling with spatial Gaussian distribution from the perspective of correlation functions. In this section, we will investigate the influence of Gaussian broadening on entanglement dynamics from the viewpoint of entanglement generation.

The numerical results in Fig. 8 presents  $C(t)$  evolution for three  $s_\mu$  values. For  $s_\mu = 0.01$  (extremely localized, close to the case of small atoms), coupling is nearly point-like, leading to weak entanglement with rapid decay. For  $s_\mu = 0.1$  (moderately localized), broader coupling introduces more photon paths, enhancing entanglement strength and stability with obvious revival. For  $s_\mu = 2$  (strongly delocalized), photons are emitted/absorbed arbitrarily across the wide region, resulting in the highest peak concurrence and robust long-term stability.

The trend in Fig. 8 is that larger  $s_\mu$  (stronger delocalization) improves entanglement performance. As the distribution width  $s_\mu$  increases, it corresponds to the transition from small atoms to giant atoms. Compared to the case of small atoms illustrated in Fig. 1(a), giant atoms offer far more diverse photon emission and absorption pathways. This creates additional opportunities for building correlations between the two atoms, thus facilitating the generation of entanglement.

### Appendix D: The influence of center position

In this section, we show the influence of the center position of the coupling distribution. In the Gaussian distribution in Eq. (32),  $\bar{x}_a$  and  $\bar{x}_b$  determine the center of the coupling profile for two giant atoms. From the numerical results in Fig. 9, in the localized coupling regime ( $s_\mu = 0.1$ ), the concurrence  $C(t)$  exhibits strong dependence on the center positions  $\bar{x}_\mu$  of the coupling distribution [Fig. 9(a)], arising from photon-mediated interactions between giant atoms. The cross-section of concurrence at  $\omega t = 0.2$  [Fig. 9(b)] clearly demonstrates spatial modulation. Actually, the residue entanglement depends on  $\Delta \bar{x}_{ab} = \bar{x}_a - \bar{x}_b$  since  $\Delta \bar{x}_{ab}$  corresponds to the phase accumulation between the photon emission and reabsorption.

In the delocalized coupling regime ( $s_\mu = 4$ ), the system exhibits markedly different behavior: Entanglement becomes highly insensitive to the center position of coupling distribution [Fig. 10(a)]. The two-dimensional concurrence profile at  $\omega t = 0.2$  versus  $\Delta \bar{x}_{ab}$  [Fig. 10(b)] shows minimal fluctuations, demonstrating exceptional robustness. This stability originates from extended coupling distributions creating multiple interaction channels between photons. Taking the photon emission-reabsorption by different atoms as an example. The photon can be emitted in any position in the region of  $g_a(x)$ , and then reabsorbed in any position in the region of  $g_b(x)$ . The phase accumulated for each possible emission-reabsorption path can be quite different, and the averaging of all trajectories has smoothed out the impact caused by the center position.

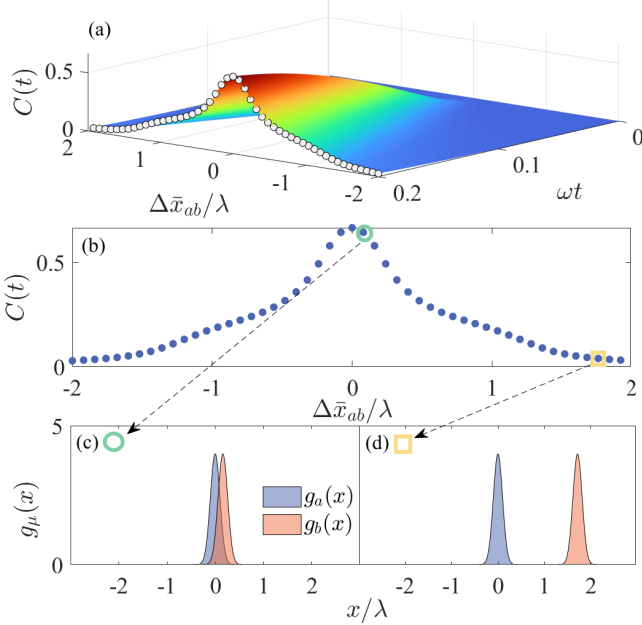


FIG. 9. Entanglement generation in localized regime ( $s_\mu = 0.1$ ). (a) Concurrence  $C(t)$  as a function of  $\Delta \bar{x}_{ab}$  and  $\omega t$ . (b) Cross-section at  $\omega t = 0.2$ . (c-d) Examples of coupling distributions at  $\Delta \bar{x}_{ab} = 0.08\lambda$  and  $\Delta \bar{x}_{ab} = 1.92\lambda$ .

#### Appendix E: Thermal initial states in waveguide

In the case of the finite-temperature waveguide, we can transform the finite temperature case into an effective zero temperature model by introducing a fictitious bath [75]. The initial thermal state of the waveguide can be written as

$$\rho_W(0) = \frac{e^{-\beta H_W}}{Z}, \quad (\text{E1})$$

where  $Z = \text{tr}[e^{-\beta H_W}]$  is the partition function with  $\beta = \frac{1}{k_B T}$ . The occupation number for mode  $k$  should be

$$\langle c_k^\dagger c_k \rangle = \frac{1}{e^{\beta \hbar \omega_k} - 1}. \quad (\text{E2})$$

This is the well known Bose-Einstein distribution. By introducing a fictitious mode with negative frequencies  $H_B = -\sum_k \omega_k b_k^\dagger b_k$ , the finite temperature problem can be mapped into a zero temperature problem. After adding a fictitious bath, the total Hamiltonian becomes

$$\begin{aligned} H_{\text{tot}} = & H_A + \sum_k \omega_k c_k^\dagger c_k + \sum_{\mu=a,b} \sum_k (g_{\mu k} c_k^\dagger \sigma_\mu^- + H.c.) \\ & - \sum_k \omega_k b_k^\dagger b_k. \end{aligned} \quad (\text{E3})$$

It should be noted that the fictitious bath  $H_B$  has no direct interaction with either the giant atoms or the waveguide. Therefore it has no impact on the dynamics of

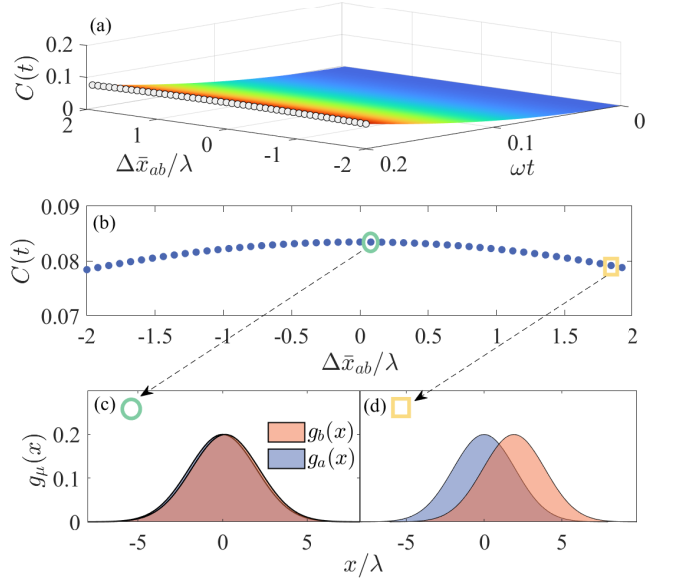


FIG. 10. Entanglement generation in delocalized regime ( $s_\mu = 4$ ). (a) Weak  $\Delta \bar{x}_{ab}$ -dependence of  $C(t)$  evolution. (b) Cross-section of  $C(t)$  at  $\omega t = 0.2$ . (c-d) Examples of coupling distributions at  $\Delta \bar{x}_{ab} = 0.08\lambda$  and  $\Delta \bar{x}_{ab} = 1.92\lambda$ .

the original Hamiltonian (system plus the original waveguide). Namely, solving this Hamiltonian is equivalent to solving the original Hamiltonian.

After a Bogoliubov transformation

$$c_k = \sqrt{\bar{n}_k + 1} d_k + \sqrt{\bar{n}_k} e_k^\dagger, \quad (\text{E4})$$

$$b_k = \sqrt{\bar{n}_k + 1} e_k + \sqrt{\bar{n}_k} d_k^\dagger, \quad (\text{E5})$$

the Hamiltonian becomes

$$\begin{aligned} H'_{\text{tot}} = & H_A + \sum_k \omega_k d_k^\dagger d_k + \sum_{\mu,k} \sqrt{\bar{n}_k + 1} (g_{\mu k} \sigma_\mu^- d_k^\dagger + H.c.) \\ & - \sum_k \omega_k e_k^\dagger e_k + \sum_{\mu,k} \sqrt{\bar{n}_k} (g_{\mu k} \sigma_\mu^- e_k + H.c.). \end{aligned} \quad (\text{E6})$$

It is easy to check the vacuum state for the system  $|0\rangle = |0\rangle_d \otimes |0\rangle_e$  satisfies  $d_k|0\rangle = 0$ , and  $e_k|0\rangle = 0$ , and it keeps the original Bose-Einstein distribution at temperature  $T$  in Eq. (E2). Therefore, solving the transformed Hamiltonian (E6) with the initial state  $|0\rangle_d \otimes |0\rangle_e$  is equivalent to solving the original Hamiltonian with the thermal initial state  $\rho_W(0) = e^{-\beta H_W}/Z$ . Thus, the finite temperature problem is transformed into a zero temperature problem. Then, following the similar procedure used in Sec. IV, one can define a stochastic state vector as  $|\psi(t, z^*, w^*)\rangle \equiv \langle z, w | \psi_{\text{tot}}(t) \rangle$ , where we use coherent states  $|z\rangle$  and  $|w\rangle$  to expand both bosonic modes  $d_k$  and

$e_k$ .

$$\begin{aligned} \frac{\partial}{\partial t} |\psi(t, z^*, w^*)\rangle &= \sum_{\substack{\mu, \nu=a, b \\ \mu \neq \nu}} \left\{ -iH_A + \sigma_\mu^- z_{\mu t}^* + \sigma_\mu^+ w_{\mu t}^* \right. \\ &\quad \left. - \sigma_\mu^+ \int_0^t ds \left[ \alpha_{\mu\mu}(t, s) \frac{\delta}{\delta z_{\mu s}^*} + \alpha_{\mu\nu}(t, s) \frac{\delta}{\delta z_{\nu s}^*} \right] \right. \\ &\quad \left. - \sigma_\mu^- \int_0^t ds \left[ \alpha'_{\mu\mu}(t, s) \frac{\delta}{\delta w_{\mu s}^*} + \alpha'_{\mu\nu}(t, s) \frac{\delta}{\delta w_{\nu s}^*} \right] \right\} |\psi(t, z^*, w^*)\rangle \end{aligned} \quad (\text{E7})$$

where  $z_{\mu t}^* = -i \sum_k \sqrt{n_k + 1} g_{\mu k} z_k^* e^{i\omega_k t}$  and  $w_{\mu t}^* = -i \sum_k \sqrt{n_k} g_{\mu k}^* w_k^* e^{-i\omega_k t}$  are statistically independent Gaussian noises.  $\alpha_{\mu\mu}(t, s) = \sum_k |f_{\mu k}|^2 e^{-i\omega_k(t-s)}$  and  $\alpha'_{\mu\mu}(t, s) = \sum_k |h_{\mu k}|^2 e^{-i\omega_k(t-s)}$  are the auto-correlation functions,  $\alpha_{\mu\nu}(t, s) = \sum_k f_{\mu k}^* f_{\nu k} e^{-i\omega_k(t-s)}$  and  $\alpha'_{\mu\nu}(t, s) = \sum_k h_{\mu k}^* h_{\nu k} e^{-i\omega_k(t-s)}$  are the cross-correlation functions with the subindex  $\mu \neq \nu$ , where  $f_{\mu k} = \sqrt{n_k + 1} g_{\mu k}$  and  $h_k = \sqrt{n_k} g_{\mu k}$ . Then, we can replace the functional derivatives in Eq. (E7) by four  $O$  operators

$$\begin{aligned} O_{z\mu}(t, s, z^*, w^*) |\psi(t, z^*, w^*)\rangle &= \frac{\delta}{\delta z_{\mu s}^*} |\psi(t, z^*, w^*)\rangle, \\ O_{w\mu}(t, s, z^*, w^*) |\psi(t, z^*, w^*)\rangle &= \frac{\delta}{\delta w_{\mu s}^*} |\psi(t, z^*, w^*)\rangle, \end{aligned} \quad (\text{E8})$$

and the  $O$  operators satisfy the following equations,

$$\begin{aligned} \frac{\partial}{\partial t} O_{z\mu} &= \sum_{\nu=a, b} \left\{ [-iH_A + \sigma_\nu^- z_{\nu t}^* + \sigma_\nu^+ w_{\nu t}^* - \sigma_\nu^+ \bar{O}_{z\nu} \right. \\ &\quad \left. - \sigma_\nu^+ \bar{O}_{w\nu}, O_{z\mu}] - \sigma_\nu^\dagger \frac{\delta}{\delta z_{\mu s}^*} \bar{O}_{z\nu} - \sigma_\nu^+ \frac{\delta}{\delta z_{\mu s}^*} \bar{O}_{w\nu} \right\}, \\ \frac{\partial}{\partial t} O_{w\mu} &= \sum_{\nu=a, b} \left\{ [-iH_A + \sigma_\nu^- z_{\nu t}^* + \sigma_\nu^+ w_{\nu t}^* - \sigma_\nu^+ \bar{O}_{z\nu} \right. \\ &\quad \left. - \sigma_\nu^+ \bar{O}_{w\nu}, O_{w\mu}] - \sigma_\nu^+ \frac{\delta}{\delta z_{\mu s}^*} \bar{O}_{z\nu} - \sigma_\nu^\dagger \frac{\delta}{\delta z_{\mu s}^*} \bar{O}_{w\nu} \right\}, \end{aligned} \quad (\text{E9})$$

with the initial conditions

$$\begin{aligned} O_{z\mu}(t, s=t, z^*, w^*) &= \sigma_\mu^-, \\ O_{w\mu}(t, s=t, z^*, w^*) &= \sigma_\mu^+. \end{aligned}$$

These equations will help us to fully determine the exact  $O$  operator for the finite-temperature case. Then, similar to the master equation (29), we can also derive the master equation for the finite-temperature case,

$$\begin{aligned} \frac{\partial}{\partial t} \rho &= -i[H_A, \rho] + \sum_{\mu=a, b} ([\sigma_\mu^-, \mathcal{M}\{P_t \bar{O}_{z\mu}^\dagger\}] + \text{H.c.}) \\ &\quad + \sum_{\mu=a, b} ([\sigma_\mu^-, \mathcal{M}\{P_t \bar{O}_{w\mu}^\dagger\}] + \text{H.c.}), \end{aligned} \quad (\text{E10})$$

where  $P_t \equiv |\psi(t, z^*, w^*)\rangle \langle \psi(t, z, w)|$  is the stochastic density operator.

## Appendix F: Squeezed initial states in waveguide

The general routine of dealing with the squeezed initial states is already set up in [76]. Considering the initial state of the waveguide is prepared in squeezed states

$$|\psi_W(0)\rangle \equiv \bigotimes_k \sum_{n_k} \frac{(-\tanh r_k)^{n_k}}{\sqrt{\cosh r_k}} \frac{\sqrt{(2n_k)!}}{2^{n_k} n_k!} |2n_k\rangle. \quad (\text{F1})$$

Assuming the giant atoms and the waveguide are separate at  $t = 0$ , i.e.,  $|\psi_{\text{tot}}(0)\rangle = |\psi_A(0)\rangle \otimes |\psi_W(0)\rangle$ , the initial value of the trajectory generally reads  $|\psi_z\rangle = \langle z|\psi_{\text{tot}}(0)\rangle = \langle z|\psi_W(0)\rangle \otimes |\psi_A(0)\rangle$ . Therefore, the inner product term  $\langle z|\psi_W(0)\rangle$  is

$$\begin{aligned} \langle z|\psi_W(0)\rangle &= \prod_k \sum_{n_k} \frac{z_k^{*2n_k}}{\sqrt{(2n_k)!}} \frac{(-\tanh r_k)^{n_k}}{\sqrt{\cosh r_k}} \frac{\sqrt{(2n_k)!}}{2^{n_k} n_k!} \\ &= \prod_k \frac{1}{\sqrt{\cosh r_k}} e^{\frac{-\tanh r_k}{2}(z_k^*)^2}. \end{aligned} \quad (\text{F2})$$

Since the inner product  $\langle z|\psi_W(0)\rangle \neq 1$ , one issue arises that the initial states of trajectories  $|\psi_z(0)\rangle$  are noise dependent. Thus, we introduce a normalized trajectory  $|\varphi_z\rangle$ , defined as

$$|\varphi_z\rangle \equiv \frac{|\psi_z\rangle}{\prod_k \frac{1}{\sqrt{\cosh r_k}} e^{\frac{-\tanh r_k}{2}(z_k^*)^2}}, \quad (\text{F3})$$

to satisfy the coincidence of the initial condition  $|\varphi_z(0)\rangle = |\psi_A(0)\rangle$ . Consequently, we obtain

$$\begin{aligned} \frac{\partial}{\partial z_k^*} |\psi_z\rangle &= \prod_{k'} \frac{1}{\sqrt{\cosh r_{k'}'}} e^{\frac{-\tanh r_{k'}'}{2}(z_{k'}^*)^2} \frac{\partial}{\partial z_k^*} |\varphi_z\rangle \\ &\quad + \prod_{k'} \frac{-\tanh r_k z_k^*}{\sqrt{\cosh r_{k'}'}} e^{\frac{-\tanh r_{k'}'}{2}(z_{k'}^*)^2} |\varphi_z\rangle. \end{aligned} \quad (\text{F4})$$

Substituting it into the Schrödinger equation, a stochastic Schrödinger equation of the normalized trajectory  $|\varphi_z\rangle$  reads

$$\begin{aligned} \frac{\partial}{\partial t} |\varphi_z\rangle &= \sum_{\mu=a, b} [-iH_A + z_{\mu t}^* \sigma_\mu^- + w_{-\mu t}^* \sigma_\mu^\dagger] \\ &\quad - i\sigma_\mu^\dagger \sum_k g_k e^{-i\omega_k t} \frac{\partial}{\partial z_k^*} |\varphi_z\rangle, \end{aligned} \quad (\text{F5})$$

where two stochastic processes are defined as, both in terms of  $z_k^*$ ,

$$\begin{aligned} z_{\mu t}^* &\equiv -i \sum_k g_{\mu k}^* z_k^* e^{i \omega_k t}, \\ w_{\mu t}^* &\equiv i \sum_k g_{\mu k} z_k^* e^{i \omega_k t} \tanh r_k, \end{aligned} \quad (\text{F6})$$

respectively. Equation (F5) indicates that the new trajectory  $|\varphi_z\rangle$  involves two noises. By taking  $r_k = 0$ , it is easy to verify that  $w_t^* = 0$ , the equations are reduced to the case without squeezed initial state. In another word, the case of vacuum initial state is a specific case of Eq. (F5).

Applying the chain rule, the term of  $\frac{\partial}{\partial z_k^*} |\varphi_z\rangle$  can be explicitly extended as a sum of two integrals for the functional derivatives with respect to the two stochastic processes, that

$$\begin{aligned} &-i \sum_k g_{\mu k} e^{-i \omega_k t} \frac{\partial}{\partial z_k^*} \\ &= -i \sum_{\substack{\mu=a,b \\ \mu \neq \nu}} \sum_k g_{\mu k} e^{-i \omega_k t} \left( \int_0^t ds \frac{\partial z_{\mu s}^*}{\partial z_k^*} \frac{\delta}{\delta z_{\mu s}^*} + \int_{-t}^0 ds \frac{\partial w_{\mu s}^*}{\partial z_k^*} \frac{\delta}{\delta w_{\mu s}^*} \right. \\ &\quad \left. + \int_0^t ds \frac{\partial z_{\nu s}^*}{\partial z_k^*} \frac{\delta}{\delta z_{\nu s}^*} + \int_{-t}^0 ds \frac{\partial w_{\nu s}^*}{\partial z_k^*} \frac{\delta}{\delta w_{\nu s}^*} \right) \\ &= - \int_0^t ds \sum_k |g_{\mu k}|^2 e^{-i \omega_k (t-s)} \frac{\delta}{\delta z_{\mu s}^*} \\ &\quad + \int_{-t}^0 ds \sum_k g_{\mu k}^2 \tanh r_k e^{-i \omega_k (t-s)} \frac{\delta}{\delta w_{\mu s}^*} \\ &\quad - \int_0^t ds \sum_k g_{\mu k} g_{\nu k}^* e^{-i \omega_k (t-s)} \frac{\delta}{\delta z_{\nu s}^*} \\ &\quad + \int_{-t}^0 ds \sum_k g_{\mu k} g_{\nu k} \tanh r_k e^{-i \omega_k (t-s)} \frac{\delta}{\delta w_{\nu s}^*} \\ &= - \int_0^t ds \alpha_{\mu \mu}(t, s) \frac{\delta}{\delta z_{\mu s}^*} - \int_{-t}^0 ds \beta_{\mu \mu}(t, s) \frac{\delta}{\delta w_{\mu s}^*}, \\ &\quad - \int_0^t ds \alpha_{\mu \nu}(t, s) \frac{\delta}{\delta z_{\nu s}^*} - \int_{-t}^0 ds \beta_{\mu \nu}(t, s) \frac{\delta}{\delta w_{\nu s}^*}, \end{aligned} \quad (\text{F7})$$

where  $\alpha_{\mu \mu}(t, s) = \sum_k |g_{\mu k}|^2 e^{-i \omega_k (t-s)}$  is the correlation function of the noise  $z_{\mu t}^*$ ,  $\beta_{\mu \mu}(t, s) = \mathcal{M}(z_{\mu t} w_{\mu s}^*) = \sum_k g_{\mu k}^2 e^{-i \omega_k (t-s)} \tanh r_k$  is the cross-correlation function between the two noises,  $\alpha_{\mu \nu}(t, s) = \mathcal{M}(z_{\nu t} w_{\mu s}^*) = \sum_k g_{\mu k} g_{\nu k}^* e^{-i \omega_k (t-s)}$  and  $\beta_{\mu \nu}(t, s) = \mathcal{M}(z_{\mu t} w_{\nu s}^*) = \sum_k g_{\mu k} g_{\nu k} e^{-i \omega_k (t-s)} \tanh r_k$  are the cross-correlation functions between the two giant atoms. Moreover, we define two to-be-determined operators  $O_{z\mu}(t, s)$  and  $O_{w\mu}(t, s)$  as

$$O_{z\mu}(t, s) |\varphi_z\rangle \equiv \frac{\delta}{\delta z_{\mu s}^*} |\varphi_z\rangle, \quad O_{w\mu}(t, s) |\varphi_z\rangle \equiv \frac{\delta}{\delta w_{\mu s}^*} |\varphi_z\rangle. \quad (\text{F8})$$

With the  $O$  operators, the linear SSE Eq. (F5) can be formally written as

$$\begin{aligned} \frac{\partial}{\partial t} |\varphi_z\rangle &= (-i H_A + z_{\mu t}^* \sigma_{\mu}^- + w_{-\mu t}^* \sigma_{\mu}^{\dagger}) |\varphi_z\rangle \\ &\quad - [\sigma_{\mu}^{\dagger} \bar{O}_{z\mu}^{\alpha}(t) + \sigma_{\mu}^{\dagger} \bar{O}_{w\mu}^{\beta}(t)] |\varphi_z\rangle, \end{aligned} \quad (\text{F9})$$

where

$$\begin{aligned} \bar{O}_{z\mu}^{\alpha}(t) &\equiv \int_0^t ds [\alpha_{\mu \mu}(t, s) O_{z\mu}(t, s) \\ &\quad + \alpha_{\mu \nu}(t, s) O_{z\nu}(t, s)], \\ \bar{O}_{w\mu}^{\beta}(t) &\equiv \int_{-t}^0 ds [\beta(t, s) O_{w\mu}(t, s) \\ &\quad + \beta_{\mu \nu}(t, s) O_{z\nu}(t, s)]. \end{aligned}$$

Here, using the consistency condition that  $\frac{\partial}{\partial t} \frac{\delta}{\delta z_{\mu s}^*} |\varphi_z\rangle = \frac{\delta}{\delta z_{\mu s}^*} \frac{\partial}{\partial t} |\varphi_z\rangle$ , the two operators  $O_{z\mu}(t, s)$  and  $O_{w\mu}(t, s)$  can be determined by two evolution equations, respectively:

$$\begin{aligned} \frac{\partial}{\partial t} O_{z\mu}(t, s) &= \sum_{\substack{\mu, \nu=a,b \\ \mu \neq \nu}} \left\{ \left[ -i H_A + z_{\mu t}^* \sigma_{\mu}^- + w_{-\mu t}^* \sigma_{\mu}^{\dagger}, O_{z\mu}(t, s) \right] \right. \\ &\quad \left. + [-\sigma_{\mu}^{\dagger} \bar{O}_{z\mu}^{\alpha}(t) - \sigma_{\mu}^{\dagger} \bar{O}_{w\mu}^{\beta}(t), O_{z\nu}(t, s)] \right. \\ &\quad \left. - \frac{\delta}{\delta z_{\mu s}^*} (\sigma_{\mu}^{\dagger} \bar{O}_{z\mu}^{\alpha}(t) + \sigma_{\mu}^{\dagger} \bar{O}_{w\mu}^{\beta}(t)) \right\}, \end{aligned} \quad (\text{F10})$$

$$\begin{aligned} \frac{\partial}{\partial t} O_{w\mu}(t, s) &= \sum_{\substack{\mu, \nu=a,b \\ \mu \neq \nu}} \left\{ \left[ -i H_A + z_{\mu t}^* \sigma_{\mu}^- + w_{-\mu t}^* \sigma_{\mu}^{\dagger}, O_{w\mu}(t, s) \right] \right. \\ &\quad \left. + [-\sigma_{\mu}^{\dagger} \bar{O}_{z\mu}^{\alpha}(t) - \sigma_{\mu}^{\dagger} \bar{O}_{w\mu}^{\beta}(t), O_{w\nu}(t, s)] \right. \\ &\quad \left. - \frac{\delta}{\delta w_{\mu s}^*} (\sigma_{\mu}^{\dagger} \bar{O}_{z\mu}^{\alpha}(t) + \sigma_{\mu}^{\dagger} \bar{O}_{w\mu}^{\beta}(t)) \right\}, \end{aligned} \quad (\text{F11})$$

with the initial condition  $O_{z\mu}(t, s = t) = \sigma_{\mu}^-$  and  $O_{w\mu}(t, s = -t) = \sigma_{\mu}^{\dagger}$ .

Moreover, it is worth noting that the initial condition  $O_{w\mu}(t, s = -t) = \sigma_{\mu}^{\dagger}$  in the above discussion indicates the nontrivial dynamics of the system.

### Spatial-dependent squeezing field

One of the interesting topic related to squeezed states in waveguide is the spatial dependence of the squeezing parameter. Inspired by Ref. [85], if we consider two squeezed fields (left- and right-propagating) are injected from both ends of the waveguide, the interference of these two fields creates a standing-wave pattern of the field quadratures, meaning an atom's position directly determines whether it probes a maximally squeezed or anti-squeezed quadrature.

Similar to Ref. [85], the dual input field can be described by the operators  $b_s(k)$ , where  $s = \pm$  represents the propagating directions. Then, the Hamiltonian should be modified as

$$H_W = \sum_{s=\pm} \int dk \omega_k b_s^\dagger(k) b_s(k), \quad (F12)$$

$$H_{\text{int}} = \sum_{\mu=a,b} \sum_{s=\pm} \int dx g_\mu(x) [\sigma_\mu^- \mathcal{E}_s^\dagger(x) + \text{H.c.}],$$

where  $\mathcal{E}_\pm(x) = \int \frac{dk}{\sqrt{2\pi}} b_s(k) e^{\pm ikx}$ , and the dispersion relation is assumed linear  $\omega_k = c|k|$ . The waveguide is initially prepared in a squeezed vacuum state resulting from injecting broadband squeezed light from both ends. We assume the squeezed state is characterized by the correlation functions

$$\langle b_s^\dagger(k) b_{s'}(k') \rangle = N_{\text{ph}} \delta_{s,s'} \delta(k - k'), \quad (F13)$$

$$\langle b_s(k) b_{s'}(k') \rangle = M_{\text{ph}} \delta_{s,-s'} e^{i\phi} \delta(k + k' - 2k_c), \quad (F14)$$

where  $k_c = \omega_0/c$  is the carrier wave vector,  $N_{\text{ph}}$  and  $M_{\text{ph}}$  satisfy  $|M_{\text{ph}}|^2 = N_{\text{ph}}(N_{\text{ph}} + 1)$  for a minimal uncertainty state, and  $\phi$  is a reference phase. The factor  $\delta_{s,-s'}$  indicates that squeezing correlates photons propagating in opposite directions, leading to spatial modulation of the field quadratures as  $\cos[k_c(x + x') + \phi]$  [85].

Next, we can apply the previously discussed SSE method for handling squeezed fields here. In the derivation, one may notice  $\langle z|b_{s,k} = z_{s,k}\langle z|$  and  $\langle z|b_{s,k}^\dagger = \frac{\partial}{\partial z_{s,k}^*}\langle z|$ , where the creation and annihilation operators are direction-dependent.

---

[1] B. Kannan, M. J. Ruckriegel, D. L. Campbell, A. Frisk Kockum, J. Braumüller, D. K. Kim, M. Kjaergaard, P. Krantz, A. Melville, B. M. Niedzielski, A. Vepsäläinen, R. Winik, J. L. Yoder, F. Nori, T. P. Orlando, S. Gustavsson, and W. D. Oliver, Waveguide quantum electrodynamics with superconducting artificial giant atoms, *Nature* **583**, 775 (2020).

[2] X.-L. Yin, Y.-H. Liu, J.-F. Huang, and J.-Q. Liao, Single-photon scattering in a giant-molecule waveguide-QED system, *Phys. Rev. A* **106**, 013715 (2022).

[3] D. Cilluffo, A. Carollo, S. Lorenzo, J. A. Gross, G. M. Palma, and F. Ciccarello, Collisional picture of quantum optics with giant emitters, *Phys. Rev. Res.* **2**, 043070 (2020).

[4] A. C. Santos and R. Bachelard, Generation of Maximally Entangled Long-Lived States with Giant Atoms in a Waveguide, *Phys. Rev. Lett.* **130**, 053601 (2023).

[5] L. Guo, A. Grimsmo, A. F. Kockum, M. Pletyukhov, and G. Johansson, Giant acoustic atom: A single quantum system with a deterministic time delay, *Phys. Rev. A* **95**, 053821 (2017).

[6] G. Andersson, B. Suri, L. Guo, T. Aref, and P. Delsing, Non-exponential decay of a giant artificial atom, *Nat. Phys.* **15**, 1123 (2019).

[7] A. González-Tudela, C. S. Muñoz, and J. I. Cirac, Engineering and Harnessing Giant Atoms in High-Dimensional Baths: A Proposal for Implementation with Cold Atoms, *Phys. Rev. Lett.* **122**, 203603 (2019).

[8] A. Soro and A. F. Kockum, Chiral quantum optics with giant atoms, *Phys. Rev. A* **105**, 023712 (2022).

[9] L. Leonforte, X. Sun, D. Valenti, B. Spagnolo, F. Illuminati, A. Carollo, and F. Ciccarello, Quantum optics with giant atoms in a structured photonic bath, *Quantum Sci. Technol.* **10**, 015057 (2024).

[10] S. Terradas-Briansó, C. A. González-Gutiérrez, F. Nori, L. Martín-Moreno, and D. Zueco, Ultrastrong waveguide QED with giant atoms, *Phys. Rev. A* **106**, 063717 (2022).

[11] A. Frisk Kockum, P. Delsing, and G. Johansson, Designing frequency-dependent relaxation rates and lamb shifts for a giant artificial atom, *Phys. Rev. A* **90**, 013837 (2014).

[12] W. Zhao and Z. Wang, Single-photon scattering and bound states in an atom-waveguide system with two or multiple coupling points, *Phys. Rev. A* **101**, 053855 (2020).

[13] L. Du, Y. Zhang, J.-H. Wu, A. F. Kockum, and Y. Li, Giant Atoms in a Synthetic Frequency Dimension, *Phys. Rev. Lett.* **128**, 223602 (2022).

[14] L. Du, L. Guo, Y. Zhang, and A. F. Kockum, Giant emitters in a structured bath with non-hermitian skin effect, *Phys. Rev. Research* **5**, L042040 (2023).

[15] W. Cheng, Z. Wang, and Y.-x. Liu, Topology and retardation effect of a giant atom in a topological waveguide, *Phys. Rev. A* **106**, 033522 (2022).

[16] M. Weng, X. Wang, and Z. Wang, Interaction and entanglement engineering in a driven-giant-atom setup with a coupled resonator waveguide, *Phys. Rev. A* **110**, 023721 (2024).

[17] W. Gu, L. Chen, Z. Yi, S. Liu, and G.-x. Li, Tunable photon-photon correlations in waveguide qed systems with giant atoms, *Phys. Rev. A* **109**, 023720 (2024).

[18] H. Yu, Z. Wang, and J.-H. Wu, Entanglement preparation and nonreciprocal excitation evolution in giant atoms by controllable dissipation and coupling, *Phys. Rev. A* **104**, 013720 (2021).

[19] A. F. Kockum, G. Johansson, and F. Nori, Decoherence-free interaction between giant atoms in waveguide quantum electrodynamics, *Phys. Rev. Lett.* **120**, 140404 (2018).

[20] J. W. Yu, K. X. Yan, Y. Qiu, J. Song, Y. H. Chen, and Y. Xia, Efficient generation of arbitrary photon-number-squeezed light via shortcuts to adiabaticity, *Opt. Express* **33**, 26356 (2025).

[21] Y. Qiu, K. X. Yan, J. H. Lin, J. Song, Y. H. Chen, and

Y. Xia, Efficient protocol for exploring the quantum interference and entanglement of dirac particles, *New J. Phys.* **27**, 084503 (2025).

[22] S. W. Xu, Z. Y. Zhang, J. T. Ye, Z. Z. Zhang, Y. Y. Guo, K. X. Yan, Y. H. Chen, and Y. Xia, Optimal robust control of cat-state qubits against parameter imperfections, *Opt. Express* **33**, 40755 (2025).

[23] Y. Xiao, Y. H. Kang, R. H. Zheng, J. Song, Y. H. Chen, and Y. Xia, Effective nonadiabatic holonomic swap gate with rydberg atoms using invariant-based reverse engineering, *Phys. Rev. A* **109**, 062610 (2024).

[24] Y. Xiao, Y. H. Kang, R. H. Zheng, Y. Liu, Y. Wang, J. Song, and Y. Xia, Precise nondestructive parity measurement of artificial atoms using a superconducting resonator and homodyne measurement, *Adv. Quantum Technol.* **6**, 2200192 (2023).

[25] K. X. Yan, Y. Qiu, Y. Xiao, Y. H. Chen, and Y. Xia, Generating three-photon rabi oscillations without a large-detuning condition, *Phys. Rev. A* **110**, 043711 (2024).

[26] K. X. Yan, Y. Qiu, Y. Xiao, J. Song, Y. H. Chen, and Y. Xia, Spontaneous emission in casimir-rabi oscillations through a weak optomechanical coupling, *Opt. Express* **33**, 39283 (2025).

[27] Z. C. Shi, J. T. Ding, Y. H. Chen, J. T. Ding, J. Song, Y. Xia, X. Yi, and F. Nori, Supervised learning for robust quantum control in composite-pulse systems, *Phys. Rev. Applied* **21**, 044012 (2024).

[28] Z. C. Shi, J. H. Wang, C. Zhang, J. Song, and Y. Xia, Universal composite pulses for robust quantum state engineering in four-level systems, *Phys. Rev. A* **109**, 022441 (2024).

[29] Y. H. Chen, Z. C. Shi, F. Nori, and Y. Xia, Error-tolerant amplification and simulation of the ultrastrong-coupling quantum rabi model, *Phys. Rev. Lett.* **133**, 033603 (2024).

[30] R. H. Zheng, S. L. Su, J. Song, W. B. Li, and Y. Xia, Thermal-dephasing-tolerant generation of mesoscopic superposition states with rydberg dressed blockade, *Phys. Rev. A* **108**, 042405 (2023).

[31] D. S. Li, Y. H. Kang, Y. H. Chen, Y. Liu, C. Zhang, Y. Wang, J. Song, and Y. Xia, One-step parity measurement of n cat-state qubits via reverse engineering and optimal control, *Phys. Rev. A* **109**, 022437 (2024).

[32] Q.-Y. Qiu, Y. Wu, and X.-Y. Lü, Collective radiance of giant atoms in non-Markovian regime, *Sci. China Phys. Mech. Astron.* **66**, 224212 (2023).

[33] Z. Y. Li and H. Z. Shen, Non-Markovian dynamics with a giant atom coupled to a semi-infinite photonic waveguide, *Phys. Rev. A* **109**, 023712 (2024).

[34] A.-L. Guo, L.-T. Zhu, G.-C. Guo, Z.-R. Lin, C.-F. Li, and T. Tu, Phonon superradiance with time delays from collective giant atoms, *Phys. Rev. A* **109**, 033711 (2024).

[35] S. L. Feng and W. Z. Jia, Manipulating single-photon transport in a waveguide-qed structure containing two giant atoms, *Phys. Rev. A* **104**, 063712 (2021).

[36] L. Du and Y. Li, Single-photon frequency conversion via a giant A-type atom, *Phys. Rev. A* **104**, 023712 (2021).

[37] Y.-T. Chen, L. Du, L. Guo, Z. Wang, Y. Zhang, Y. Li, and J.-H. Wu, Nonreciprocal and chiral single-photon scattering for giant atoms, *Commun. Phys.* **5**, 215 (2022).

[38] J. Zhou, X.-L. Yin, and J.-Q. Liao, Chiral and nonreciprocal single-photon scattering in a chiral-giant-molecule waveguide-qed system, *Phys. Rev. A* **107**, 063703 (2023).

[39] A. Carollo, D. Cilluffo, and F. Ciccarello, Mechanism of decoherence-free coupling between giant atoms, *Phys. Rev. Res.* **2**, 043184 (2020).

[40] L. Du, L. Guo, and Y. Li, Complex decoherence-free interactions between giant atoms, *Phys. Rev. A* **107**, 023705 (2023).

[41] A. Soro, C. S. Muñoz, and A. F. Kockum, Interaction between giant atoms in a one-dimensional structured environment, *Phys. Rev. A* **107**, 013710 (2023).

[42] S. Guo, Y. Wang, T. Purdy, and J. Taylor, Beyond spontaneous emission: Giant atom bounded in the continuum, *Phys. Rev. A* **102**, 033706 (2020).

[43] X. Zhang, C. Liu, Z. Gong, and Z. Wang, Quantum interference and controllable magic cavity QED via a giant atom in a coupled resonator waveguide, *Phys. Rev. A* **108**, 013704 (2023).

[44] L. Guo, A. F. Kockum, F. Marquardt, and G. Johansson, Oscillating bound states for a giant atom, *Phys. Rev. Res.* **2**, 043014 (2020).

[45] X. Wang, T. Liu, A. F. Kockum, H.-R. Li, and F. Nori, Tunable chiral bound states with giant atoms, *Phys. Rev. Lett.* **126**, 043602 (2021).

[46] C. Vega, M. Bello, D. Porras, and A. González-Tudela, Qubit-photon bound states in topological waveguides with long-range hoppings, *Phys. Rev. A* **104**, 053522 (2021).

[47] K. H. Lim, W.-K. Mok, and L.-C. Kwek, Oscillating bound states in non-markovian photonic lattices, *Phys. Rev. A* **107**, 023716 (2023).

[48] R. Huang, A. Miranowicz, J.-Q. Liao, F. Nori, and H. Jing, Nonreciprocal Photon Blockade, *Phys. Rev. Lett.* **121**, 153601 (2018).

[49] Q. Y. Cai and W. Z. Jia, Coherent single-photon scattering spectra for a giant-atom waveguide-QED system beyond the dipole approximation, *Phys. Rev. A* **104**, 033710 (2021).

[50] S.-Y. Li, Z.-Q. Zhang, L. Du, Y. Li, and H. Wu, Single-photon scattering in giant-atom waveguide systems with chiral coupling, *Phys. Rev. A* **109**, 063703 (2024).

[51] K. Lalumière, B. C. Sanders, A. F. van Loo, A. Fedorov, A. Wallraff, and A. Blais, Input-output theory for waveguide QED with an ensemble of inhomogeneous atoms, *Phys. Rev. A* **88**, 043806 (2013).

[52] D. Mukhopadhyay and G. S. Agarwal, Multiple Fano interferences due to waveguide-mediated phase coupling between atoms, *Phys. Rev. A* **100**, 013812 (2019).

[53] A. M. Vadiraj, A. Ask, T. G. McConkey, I. Nsanzineza, C. W. S. Chang, A. F. Kockum, and C. M. Wilson, Engineering the level structure of a giant artificial atom in waveguide quantum electrodynamics, *Phys. Rev. A* **103**, 023710 (2021).

[54] X.-L. Yin and J.-Q. Liao, Generation of two-giant-atom entanglement in waveguide-qed systems, *Phys. Rev. A* **108**, 023728 (2023).

[55] X.-L. Yin, W.-B. Luo, and J.-Q. Liao, Non-Markovian disentanglement dynamics in double-giant-atom waveguide-QED systems, *Phys. Rev. A* **106**, 063703 (2022).

[56] X. Li, W. Zhao, and Z. Wang, Controlling photons by phonons via giant atom in a waveguide QED setup, *Opt. Lett.* **48**, 3595 (2023).

[57] M. Cheng, G. Cai, and X. Ma, Spontaneous emission dynamics of giant atom controlled by quantum coherent feedback, *Sci. China Phys. Mech. Astron.* **53**, 110311 (2023).

[58] F. Roccati and D. Cilluffo, Controlling markovianity with chiral giant atoms, *Phys. Rev. Lett.* **133**, 063603 (2024).

[59] H. Zhu, X.-L. Yin, and J.-Q. Liao, Single-photon scattering in giant-atom topological-waveguide-qed systems, *Phys. Rev. A* **111**, 023711 (2025).

[60] X.-L. Yin, H.-w. J. Lee, and G. Zhang, Giant-atom dephasing dynamics and entanglement generation in a squeezed vacuum reservoir, *Phys. Rev. A* **111**, 033707 (2025).

[61] L. Diósi, N. Gisin, and W. T. Strunz, Non-Markovian quantum state diffusion, *Phys. Rev. A* **58**, 1699 (1998).

[62] W. T. Strunz, L. Diósi, and N. Gisin, Open System Dynamics with Non-Markovian Quantum Trajectories, *Phys. Rev. Lett.* **82**, 1801 (1999).

[63] T. Yu, L. Diósi, N. Gisin, and W. T. Strunz, Non-Markovian quantum-state diffusion: Perturbation approach, *Phys. Rev. A* **60**, 91 (1999).

[64] L. Chen, D. I. G. Bennett, and A. Eisfeld, Calculating nonlinear response functions for multidimensional electronic spectroscopy using dyadic non-Markovian quantum state diffusion, *J. Chem. Phys.* **157**, 114104 (2022).

[65] X. Gao and A. Eisfeld, Charge and energy transfer in large molecular assemblies: Quantum state diffusion with an adaptive basis, *J. Chem. Phys.* **150**, 234115 (2019).

[66] J. Jing, X. Zhao, J. Q. You, and T. Yu, Time-local quantum-state-diffusion equation for multilevel quantum systems, *Phys. Rev. A* **85**, 042106 (2012).

[67] X. Zhao, J. Jing, B. Corn, and T. Yu, Dynamics of interacting qubits coupled to a common bath: Non-Markovian quantum-state-diffusion approach, *Phys. Rev. A* **84**, 032101 (2011).

[68] X. Zhao, W. Shi, L.-A. Wu, and T. Yu, Fermionic stochastic Schrödinger equation and master equation: An open-system model, *Phys. Rev. A* **86**, 032116 (2012).

[69] X. Zhao, W. Shi, J. You, and T. Yu, Non-Markovian dynamics of quantum open systems embedded in a hybrid environment, *Ann. Phys.* **381**, 121 (2017).

[70] X. Zhao, Macroscopic entanglement in optomechanical system induced by non-Markovian environment, *Opt. Express* **27**, 29082 (2019).

[71] X. Zhao, Y.-h. Ma, and Y. Xia, Noise-assisted quantum coherence protection in a hierarchical environment, *Phys. Rev. A* **105**, 042217 (2022).

[72] X. Zhao and Y. Xia, Non-Markovian environment induced Schrödinger cat state transfer in an optical Newton's cradle, *Opt. Express* **33**, 619 (2025).

[73] Y.-L. Xiang, X. Zhao, and Y. Xia, Non-markovian-environment-induced chaos in an optomechanical system, *Physical Review A* **112**, 10.1103/knfq-17nw (2025).

[74] Y. L. Xiang, X. Y. Zhao, and Y. Xia, Chaotic behavior in optomechanical system embedded in non-markovian environment, *Laser Phys.* **35**, 045204 (2025).

[75] T. Yu, Non-Markovian quantum trajectories versus master equations: Finite-temperature heat bath, *Phys. Rev. A* **69**, 062107 (2004).

[76] W. Shi, Q. Ding, and Y. Chen, Non-Markovian open quantum dynamics in squeezed environments: Coherent-state unraveling, *Phys. Rev. A* **108**, 012206 (2023).

[77] X. Wang, H.-B. Zhu, T. Liu, and F. Nori, Realizing quantum optics in structured environments with giant atoms, *Phys. Rev. Res.* **6**, 013279 (2024).

[78] D. D. Noachtar, J. Knörzer, and R. H. Jonsson, Nonperturbative treatment of giant atoms using chain transformations, *Phys. Rev. A* **106**, 013702 (2022).

[79] W. T. Strunz and T. Yu, Convolutionless Non-Markovian master equations and quantum trajectories: Brownian motion, *Phys. Rev. A* **69**, 052115 (2004).

[80] Y. Chen, J. Q. You, and T. Yu, Exact non-markovian master equations for multiple qubit systems: Quantum-trajectory approach, *Phys. Rev. A* **90**, 052104 (2014).

[81] W. K. Wootters, Entanglement of Formation of an Arbitrary State of Two Qubits, *Phys. Rev. Lett.* **80**, 2245 (1998).

[82] C.-F. Kam and X. Hu, Fast and high-fidelity dispersive readout of a spin qubit with squeezed microwave and resonator nonlinearity, *npj Quantum Inf.* **10**, 133 (2024).

[83] W. Qin, A. Miranowicz, and F. Nori, Beating the 3 dB Limit for Intracavity Squeezing and Its Application to Nondemolition Qubit Readout, *Phys. Rev. Lett.* **129**, 123602 (2022).

[84] W. Qin, A. Miranowicz, P.-B. Li, X.-Y. Lü, J. You, and F. Nori, Exponentially Enhanced Light-Matter Interaction, Cooperativities, and Steady-State Entanglement Using Parametric Amplification, *Phys. Rev. Lett.* **120**, 093601 (2018).

[85] R. Gutiérrez-Jáuregui, A. Asenjo-García, and G. S. Agarwal, Dissipative stabilization of dark quantum dimers via squeezed vacuum, *Phys. Rev. Res.* **5**, 013127 (2023).

[86] J. Xu, X. Zhao, J. Jing, L.-A. Wu, and T. Yu, Perturbation methods for the non-Markovian quantum state diffusion equation, *J. Phys. A: Math. Theor.* **47**, 435301 (2014).